Monthly Notices
of the
ROYAL ASTRONOMICAL SOCIETY

MNRAS **481,** 860–877 (2018)
Advance Access publication 2018 August 29

doi:10.1093/mnras/sty2286

The case for a cold dark matter cusp in Draco

J. I. Read [1]★ M. G. Walker [2] and P. Steger[3]

[1]*Department of Physics, University of Surrey, Guildford, GU2 7XH, UK*
[2]*McWilliams Center for Cosmology, Department of Physics, Carnegie Mellon University, 5000 Forbes Ave., Pittsburgh, PA 15213, USA*
[3]*Department of Physics, Institute for Astronomy, ETH Zürich, Wolfgang-Pauli-Strasse 27, CH-8093 Zürich, Switzerland*

Accepted 2018 August 17. Received 2018 August 17; in original form 2018 March 15

ABSTRACT

We use a new mass modelling method, GravSphere, to measure the central dark matter density profile of the Draco dwarf spheroidal galaxy. Draco's star formation shut down long ago, making it a prime candidate for hosting a 'pristine' dark matter cusp, unaffected by stellar feedback during galaxy formation. We first test GravSphere on a suite of tidally stripped mock 'Draco'-like dwarfs. We show that we are able to correctly infer the dark matter density profile of both cusped and cored mocks within our 95 per cent confidence intervals. While we obtain only a weak inference on the logarithmic slope of these density profiles, we are able to obtain a robust inference of the amplitude of the inner dark matter density at 150 pc, $\rho_{\rm DM}(150\,{\rm pc})$. We show that, combined with constraints on the density profile at larger radii, this is sufficient to distinguish a Λ Cold Dark Matter (ΛCDM) cusp – that has $\rho_{\rm DM}(150\,{\rm pc}) \gtrsim 1.8 \times 10^8\,{\rm M}_\odot\,{\rm kpc}^{-3}$ – from alternative dark matter models that have lower inner densities. We then apply GravSphere to the real Draco data. We find that Draco has an inner dark matter density of $\rho_{\rm DM}(150\,{\rm pc}) = 2.4^{+0.5}_{-0.6} \times 10^8\,{\rm M}_\odot\,{\rm kpc}^{-3}$, consistent with a ΛCDM cusp. Using a velocity-independent SIDM model, calibrated on ΛSIDM cosmological simulations, we show that Draco's high central density gives an upper bound on the SIDM cross-section of $\sigma/m < 0.57\,{\rm cm}^2\,{\rm g}^{-1}$ at 99 per cent confidence. We conclude that the inner density of nearby dwarf galaxies like Draco provides a new and competitive probe of dark matter models.

Key words: galaxies: dwarf – galaxies: haloes – galaxies: kinematics dynamics – dark matter – cosmology: observations.

1 INTRODUCTION

The standard ΛCDM cosmological gives an excellent description of the cosmic microwave background radiation (e.g. Planck Collaboration et al. 2014), the growth of structure on large scales (e.g. Springel, Frenk & White 2006; Baur et al. 2016), and the offsets between mass and light in weak lensing systems (e.g. Clowe et al. 2006; Harvey et al. 2015). Yet, it contains two mysterious ingredients – dark matter and dark energy – that remain elusive. One path to constraining the nature of dark matter is to probe its distribution on ever smaller scales, where ΛCDM is less well-tested and where differences between competing dark matter models are maximized (e.g. Spergel & Steinhardt 2000; Bode, Ostriker & Turok 2001; Baur et al. 2016). This 'near-field cosmology' showed early promise, turning up a host of 'small-scale puzzles' that continue to challenge ΛCDM today (e.g. Bullock & Boylan-Kolchin 2017). The oldest of these is the 'cusp–core' problem: the inner rotation curves of dwarf irregular galaxies rise less steeply than expected from pure dark matter structure formation simulations (Moore 1994; Flores & Primack 1994). This implies that the central dark matter density of these dwarfs is lower than expected in a pure–dark matter ΛCDM cosmology.

Many solutions have been proposed for the cusp–core problem, falling into three main classes. The first class changes the nature of dark matter itself. Such models include 'Self-Interacting Dark Matter' (SIDM; Spergel & Steinhardt 2000; Rocha et al. 2013; Elbert et al. 2015; Kaplinghat, Tulin & Yu 2016; Robles et al. 2017; Schneider et al. 2017); 'Warm Dark Matter' (e.g. Avila-Reese et al. 2001; Bode et al. 2001; Dalcanton & Hogan 2001; Lovell et al. 2014; Schneider et al. 2017, but see Macciò et al. 2012 and Shao et al. 2013); 'fuzzy DM' (Hu, Barkana & Gruzinov 2000), 'fluid' DM (Peebles 2000), and 'wave-like' DM (Schive, Chiueh & Broadhurst 2014), to name a few. The second class invokes some problem with the data, arguing that the measurements are wrong because of poor resolution (e.g. de Blok 2010), incorrectly measured inclinations (e.g. Rhee et al. 2004; Read et al. 2016b), disequilibrium (e.g. Read et al. 2016b), unmodelled pressure support (e.g. Rhee et al. 2004; Valenzuela et al. 2007; Pineda et al. 2017), or unmodelled

★ E-mail: justin.inglis.read@gmail.com

triaxiality/non-circular motions (e.g. Rhee et al. 2004; Valenzuela et al. 2007; Kuzio de Naray & Kaufmann 2011; Oman et al. 2017). The third class invokes missing 'baryonic physics'. In this, the gravitational interaction between normal 'baryonic' matter (stars and gas) – that are not included in the pure dark matter simulations discussed above – physically transforms the dark matter cusp to a core (e.g. Navarro, Eke & Frenk 1996a; El-Zant, Shlosman & Hoffman 2001; Read & Gilmore 2005; Del Popolo 2009; Goerdt et al. 2010; Pontzen & Governato 2012; Nipoti & Binney 2015).

Of the three solutions, above, the first is the most exciting as it reveals to us something about the nature of dark matter. However, for this to be convincing, the other two classes must first be ruled out. Much work has gone into probing the second class of solution (e.g. Valenzuela et al. 2007; Kuzio de Naray & Kaufmann 2011; Read et al. 2016b; Pineda et al. 2017), typically by applying standard techniques to mock data. While individual cases can be found where the standard techniques fail, none of the potential problems discussed to date would systematically bias all dwarfs towards apparent dark matter cores. Yet, this is what is needed to explain the data (e.g. Pineda et al. 2017; Allaert, Gentile & Baes 2017).

The third solution, however, has proven more promising. Navarro et al. (1996a) were the first to suggest that impulsive gas blow out could irreversibly heat dark matter in dwarf galaxies. For a single burst, the effect is small (Gnedin & Zhao 2002). However, multiple bursts can gradually transform a cusp to a core (Read & Gilmore 2005). Such an effect is now seen in simulations of dwarf galaxies that resolve the clumpy interstellar medium (e.g. Mashchenko, Wadsley & Couchman 2008; Pontzen & Governato 2012, 2014). Furthermore, these simulations make several testable predictions: (i) star formation should be bursty with a duty cycle comparable to the local dynamical time, and a peak-to-trough ratio of 5−10 (Teyssier et al. 2013); (ii) stars should be similarly heated along with the dark matter, leading to a 'hot' stellar distribution with $v/\sigma \sim 1$, where v is the rotational velocity and σ is the velocity dispersion (Read & Gilmore 2005; Leaman et al. 2012; Teyssier et al. 2013); (iii) dark matter cores should have a size of the order of the projected half stellar mass radius, $R_{1/2}$ (Oñorbe et al. 2015; Read, Agertz & Collins 2016a); and (iv) galaxies that stopped forming stars long ago should be cuspier than those that formed stars for a Hubble time (Peñarrubia et al. 2012; Di Cintio et al. 2014; Oñorbe et al. 2015; Read et al. 2016a). Predictions (i)–(iii) have now all been tested against real data and passed (Leaman et al. 2012; Kauffmann 2014; El-Badry et al. 2016; Allaert et al. 2017; Read et al. 2017; Sparre et al. 2017; Wheeler et al. 2017). However, prediction (iv) remains elusive. The challenge is to measure the central dark matter density profile in a galaxy that is no longer star forming today. However, such galaxies are, by construction, devoid of HI gas and so we can no longer use a rotation curve to reconstruct their mass distribution. Instead, we must make use of the velocities of their individual stars. This is made difficult by the '$\rho-\beta$ degeneracy' (e.g. Binney & Mamon 1982; Merrifield & Kent 1990; Read & Steger 2017). This is a degeneracy between the radial density profile, $\rho(r)$, and the unknown orbit distribution of the stars. This latter is typically parameterized by the 'velocity anisotropy parameter', $\beta(r)$ (equation (11)), which is hard to constrain with line-of-sight velocities alone (e.g. Read & Steger 2017).

Several methods have been proposed to break the $\rho-\beta$ degeneracy, including modelling multiple populations of different scale lengths all moving with the same potential (e.g. Battaglia et al. 2008; Walker & Peñarrubia 2011; Zhu et al. 2016), using higher order velocity moments (e.g. Łokas 2009), Schwarzschild methods (e.g. Breddels et al. 2013; Jardel et al. 2013), proper motions (Strigari, Bullock & Kaplinghat 2007; Massari et al. 2018), and 'Virial Shape Parameters' (VSPs; Merrifield & Kent 1990; Richardson & Fairbairn 2014; Read & Steger 2017). In this paper, we use this latter method, implemented in the non-parametric Jeans modelling code, GravSphere (Read & Steger 2017). This has the advantages that: (i) only line of sight velocity data are required; (ii) we need make no assumption about the form of the velocity distribution function; and (iii) no population splitting is required (Read & Steger 2017). We focus on modelling the dark matter distribution in the Draco dwarf spheroidal galaxy (dSph). Draco was first discovered by Wilson (1955) using photographic plates. It lies just 76 kpc from the Galactic centre and, with a stellar mass of $M_* = 0.29 \times 10^6\,\mathrm{M}_\odot$, is one of the most dark-matter-dominated galaxies in the Universe (e.g. Kleyna et al. 2001; McConnachie 2012). Draco is particularly interesting because it stopped forming stars ∼10 Gyrs ago (Aparicio, Carrera & Martínez-Delgado 2001). This makes it a prime candidate for hosting a 'pristine' dark matter cusp within its projected stellar half light radius, $R_{1/2} = 0.22$ kpc (McConnachie 2012), unaffected by bursty star formation (e.g. Brook & Di Cintio 2015; Read et al. 2016a; Bermejo-Climent et al. 2018). However, unlike other galaxies with similarly old-age stellar populations, Draco also has a large number of ∼500 member stars with well-measured radial velocities (Walker, Olszewski & Mateo 2015a). We will show in Section 4 that this is sufficient to break the $\rho-\beta$ degeneracy and measure the inner dark matter density, even if Draco has experienced tidal stripping by the Milky Way down to its projected half stellar mass radius, $R_{1/2}$.

This paper is organized as follows. In Section 2, we briefly review the cusp–core problem in ΛCDM. We show that, while the cusp–core problem is usually framed in terms of the inner logarithmic slope of the density profile, the amplitude of the central density – that is easier to determine observationally – is sufficient to constrain interesting models like SIDM. In Section 3, we briefly describe the GravSphere method; a more complete description, including a large number of tests is given in Read & Steger (2017). We also describe our SIDM model and its calibration on ΛSIDM simulations (Section 3.2). In Section 4, we test GravSphere on a suite of tidally stripped mock 'Draco'-like dwarfs, showing that we are able to recover the dark matter density profile of these mocks within our 95 per cent confidence intervals. In Section 5, we describe our data compilation and reduction for Draco. In Section 6, we present our results by applying GravSphere to these data. We show that our GravSphere models for Draco favour a large central density, consistent with a dark matter cusp and we use this to to place a new constraint on the self-interaction cross section of dark matter. In Section 7, we discuss the caveats inherent in our modelling and the implications of our results in the context of ΛCDM. Finally, in Section 8, we present our conclusions.

2 THE CUSP–CORE PROBLEM IN ΛCDM

Pure dark matter simulations in ΛCDM predict halos that have a density profile that is well-fit (at the ∼10 per cent level[1]) by a split-power law known as the 'Navarro, Frenk & White' (NFW) profile (Navarro, Frenk & White 1996b):

$$\rho_{\rm NFW}(r) = \rho_0 \left(\frac{r}{r_s}\right)^{-1} \left(1 + \frac{r}{r_s}\right)^{-2}, \quad (1)$$

[1]An Einasto profile provides a slightly better fit (e.g. Merritt et al. 2006), though even this can be improved upon (e.g. Stadel et al. 2009). The classic NFW profile will suffice for our study here.

where the central density ρ_0 and scale length r_s are given by:

$$\rho_0 = \rho_{\rm crit}\Delta c_{200}^3 g_c/3 \;\;;\;\; r_s = r_{200}/c_{200}, \tag{2}$$

$$g_c = \frac{1}{\log(1+c_{200}) - \frac{c_{200}}{1+c_{200}}}, \tag{3}$$

and

$$r_{200} = \left[\frac{3}{4} M_{200}\frac{1}{\pi\,\Delta\rho_{\rm crit}}\right]^{1/3}, \tag{4}$$

where c_{200} is the dimensionless *concentration parameter*; $\Delta = 200$ is the over-density parameter; $\rho_{\rm crit} = 136.05\,{\rm M}_\odot\,{\rm kpc}^{-3}$ is the critical density of the Universe at redshift $z = 0$; r_{200} is the 'virial' radius at which the mean enclosed density is $\Delta \times \rho_{\rm crit}$; and M_{200} is the 'virial' mass – the mass within r_{200}.

The mass and concentration of halos in ΛCDM are correlated. Dutton & Macciò (2014) find a best-fitting relation for field halos of:

$$\log_{10}(c_{200}) = 0.905 - 0.101\log_{10}(M_{200}h - 12) \tag{5}$$

with scatter $\Delta\log_{10}(c_{200}) = 0.1$, where $h \sim 0.7$ is the Hubble parameter. (Note that subhalos are found to be more concentrated than field halos, most likely due to tidal stripping steepening their outer density profiles, e.g. Springel et al. 2008 and Klypin, Trujillo-Gomez & Primack 2011. We will consider this further in Section 3.2.)

While pure dark matter simulations in ΛCDM predict dense central cusps, modern simulations that include the effects of gas cooling, star formation, and feedback find that – provided sufficient star formation takes place – these dense cusps are transformed to cores in the centres of dwarf galaxies (see Section 1). Read et al. (2016a) parameterize this transformation with the 'coreNFW' profile that has a cumulative mass given by:

$$M_{\rm cNFW}(<r) = M_{\rm NFW}(<r)f^n, \tag{6}$$

where $M_{\rm NFW}(<r)$ is the cumulative mass of the NFW profile:

$$M_{\rm NFW}(r) = M_{200}g_c\left[\ln\left(1+\frac{r}{r_s}\right) - \frac{r}{r_s}\left(1+\frac{r}{r_s}\right)^{-1}\right] \tag{7}$$

and the function f^n generates a shallower profile below a core-size parameter, r_c:

$$f^n = \left[\tanh\left(\frac{r}{r_c}\right)\right]^n. \tag{8}$$

The density profile of this coreNFW model is given by:

$$\rho_{\rm cNFW}(r) = f^n\rho_{\rm NFW} + \frac{nf^{n-1}(1-f^2)}{4\pi r^2 r_c}M_{\rm NFW}. \tag{9}$$

Read et al. (2016a) find that their dark matter density profiles become visibly cored below $R_{1/2}$, which corresponds to a core size parameter of $r_c = 1.75R_{1/2}$. For this reason, we define here a 'visible core size parameter', $r_{cv} \equiv r_c/1.75$. Other groups using different simulation codes and sub-grid physics recipes have found similar results (e.g. Di Cintio et al. 2014 and Oñorbe et al. 2015). Indeed, Schneider et al. (2017) and Allaert et al. (2017) show that the two main fitting functions proposed in the literature to date – the coreNFW profile, above, and the Di Cintio et al. 2014 profile – produce near-identical results when applied to both simulated and real data.

In Fig. 1, we show the inner dark matter density as a function of halo mass M_{200} for four different halo models. We define 'inner' to be 150 pc which is $\sim 0.75R_{1/2}$ for Draco (see Section 5). This

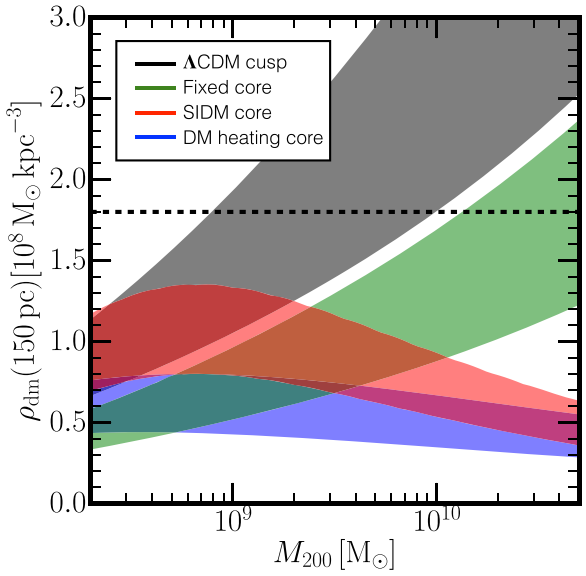

Figure 1. Dark matter cusps in ΛCDM have a high central density. This plot shows the dark matter density at 150 pc ($\rho_{\rm DM}(150\,{\rm pc})$) as a function of halo mass M_{200} for four different models. The grey band is for predictions from pure dark matter simulations in an ΛCDM cosmology (i.e. NFW profiles; equation (1)). The width of the band owes to the expected 1σ scatter in the mass–concentration relation (equation (5)). The green band marks the same but for a coreNFW profile with a fixed visible core size of $r_{cv} = 250\,{\rm pc}$. The red band shows the halos in a SIDM model with a self-interaction cross-section of $\sigma/m = 0.25\,{\rm cm}^2/{\rm g}$ (see Section 3.2 for details of this model). The blue band shows a model in which dark matter is 'heated up' by bursty star formation, assuming that there has been sufficient star formation for core formation to complete (Di Cintio et al. 2014; Oñorbe et al. 2015; Read et al. 2016a). Notice that, for plausible pre-infall halo masses for Draco (10^9–$10^{10}\,{\rm M}_\odot$), a single measurement of $\rho_{\rm DM}(150\,{\rm pc}) > 1.8\times10^8\,{\rm M}_\odot\,{\rm kpc}^{-3}$ (horizontal dashed line) would imply that Draco has a visible core size $r_{cv} \lesssim 250\,{\rm pc}$, favouring the cusped models (grey band) over the SIDM and 'dark matter heating' cored models.

is a compromise between picking a radius that is inside $R_{1/2}$, but not so small that we are not able to constrain the dark matter density observationally. The grey band shows predictions from pure dark matter simulations in an ΛCDM cosmology (i.e. NFW profiles; equation (1)). The width of the band owes to the expected 1σ scatter in the mass-concentration relation (equation (5)). The green band marks the same but for a coreNFW profile with a fixed visible core size of $r_{cv} = 250\,{\rm pc}$. The red band shows the halos in an SIDM model with a self-interaction cross-section of $\sigma/m = 0.25\,{\rm cm}^2/{\rm g}$ (see Section 3.2 for details of this model). The blue band shows the expectation for models in which dark matter is 'heated up' by bursty star formation, assuming complete core formation (i.e. a full Hubble time of star formation). In this case, the dark matter core size is expected to scale with the projected half light radius of the stars, $R_{1/2}$ (Di Cintio et al. 2014; Oñorbe et al. 2015; Read et al. 2016a). Since $R_{1/2} \sim 0.015\,r_{200}$ (Kravtsov 2013), this gives a visible core size of $r_{cv} = 0.015\,r_{200}$. Notice that for plausible pre-infall halo masses for Draco ($M_{200} = 10^9$–$10^{10}\,{\rm M}_\odot$), a single measurement of $\rho_{\rm DM}(150\,{\rm pc}) > 1.8\times10^8\,{\rm M}_\odot\,{\rm kpc}^{-3}$ (horizontal dashed line) would imply that Draco has a visible core size $r_{cv} \lesssim 250{\rm pc}$, favouring the cusped models (grey band) over the SIDM and 'dark matter heating' cored models (red, green, and blue bands).

Many studies of the cusp–core problem have focussed on measuring the logarithmic slope of the density profile, $\gamma_{\rm DM}(r) \equiv d$

$\ln \rho_{\rm DM}/d \ln r(r)$, or the asymptotic slope $\gamma_{\rm DM}(r \to 0)$. Both of these are challenging to measure, as we shall show in Section 4. However, as can be seen in Fig. 1, the amplitude of the central density, combined with information on $\rho_{\rm DM}(r)$ at larger radii, is already sufficient to distinguish interesting cosmological models, for example SIDM (Section 3.2) or models in which a central dark matter core forms in response to stellar feedback.

3 METHOD

3.1 GravSphere

GravSphere is described and tested in detail in Read & Steger (2017). It solves the projected spherical Jeans equation (Jeans 1922; Binney & Mamon 1982):

$$\sigma^2_{\rm LOS}(R) = \frac{2}{\Sigma(R)} \int_R^\infty \left(1-\beta\frac{R^2}{r^2}\right) \nu\sigma_r^2 \frac{r\,{\rm d}r}{\sqrt{r^2-R^2}}\,, \tag{10}$$

where $\Sigma(R)$ denotes the tracer surface mass density at projected radius R; $\nu(r)$ is the spherically averaged tracer density; and $\beta(r)$ is the velocity anisotropy:

$$\beta = 1 - \frac{\sigma_t^2}{\sigma_r^2}, \tag{11}$$

where σ_t and σ_r are the tangential and radial velocity dispersions, respectively, and σ_r is given by (van der Marel 1994; Mamon & Łokas 2005):

$$\sigma_r^2(r) = \frac{1}{\nu(r)g(r)} \int_r^\infty \frac{GM(\tilde{r})\nu(\tilde{r})}{\tilde{r}^2} g(\tilde{r}){\rm d}\tilde{r} \tag{12}$$

where:

$$g(r) = \exp\left(2\int \frac{\beta(r)}{r}{\rm d}r\right) \tag{13}$$

and $M(r)$ is the cumulative mass of the dwarf galaxy (due to all stars, gas, dark matter etc.).

GravSphere uses a free-form, or 'non-parametric', model for $M(r)$ that comprises a contribution from all visible matter and a contribution from dark matter that is described by a sequence of power laws defined on a set of radial bins. In this paper, these bins are defined at [0.25, 0.5, 1, 2, 4]$R_{1/2}$ where $R_{1/2}$ is the projected half light radius of the tracer stars. The tracer light profile is also non-parametric, using a series sum of Plummer spheres, as in Rojas-Niño et al. (2016). The velocity anisotropy is given by a form that makes $g(r)$ analytic:

$$\beta(r) = \beta_0 + (\beta_\infty - \beta_0)\,\frac{1}{1+\left(\frac{r_0}{r}\right)^n}, \tag{14}$$

where β_0 is the inner asymptotic anisotropy, β_∞ is the outer asymptotic anisotropy, r_0 is a transition radius, and n controls the sharpness of the transition.

To avoid infinities in β for highly tangential orbits, for model fitting we use a symmetrized $\tilde{\beta}$ (Read et al. 2006b; Read & Steger 2017):

$$\tilde{\beta} = \frac{\sigma_r^2 - \sigma_t^2}{\sigma_r^2 + \sigma_t^2} = \frac{\beta}{2-\beta}, \tag{15}$$

where $\tilde{\beta} = -1$ corresponds to full tangential anisotropy; $\tilde{\beta} = 1$ to full radial anisotropy; and $\tilde{\beta} = 0$ to isotropy. We assume flat priors on $-1 < \tilde{\beta}_{0,\infty} < 1$ such that we give equal weight to tangentially and radially anisotropic models.

By default, GravSphere also fits for the two higher order 'Virial Shape Parameters' (VSPs; Merrifield & Kent 1990; Richardson & Fairbairn 2014; Read & Steger 2017):

$$v_{s1} = \frac{2}{5}\int_0^\infty GM\,(5-2\beta)\,\nu\sigma_r^2\,r\,{\rm d}r \tag{16}$$

$$= \int_0^\infty \Sigma\langle v^4_{\rm LOS}\rangle\,R\,{\rm d}R \tag{17}$$

$$v_{s2} = \frac{4}{35}\int_0^\infty GM\,(7-6\beta)\,\nu\sigma_r^2\,r^3\,{\rm d}r \tag{18}$$

$$= \int_0^\infty \Sigma\langle v^4_{\rm LOS}\rangle\,R^3\,{\rm d}R\,. \tag{19}$$

These VSPs involve fourth-order moments of the line-of-sight velocities $\langle v^4_{\rm LOS}\rangle$, but depend only on β and not on its fourth-order counterparts (Merrifield & Kent 1990; Richardson & Fairbairn 2014; Read & Steger 2017). Thus, v_{s1} and v_{s2} allow us to obtain constraints on β via line-of-sight velocities alone, breaking the $\rho-\beta$ degeneracy (e.g. Binney & Mamon 1982; Merrifield & Kent 1990; Read & Steger 2017). We use VSPs in our modelling throughout this paper.

We introduce a key improvement in our estimators for v_{s1} and v_{s2} as compared to Read & Steger (2017). In Read & Steger (2017), we assumed that $\langle v^4_{\rm LOS}\rangle$ is zero wherever we have no data. This can lead to bias in v_{s1} and v_{s2} if $\langle v^4_{\rm LOS}\rangle$ is flat or rising beyond the outermost datapoint, $R_{\rm data}$. To improve on this, we fit a power law to $\langle v^4_{\rm LOS}\rangle$ over all radii $R > R_{1/2}$, using this to extrapolate its large R behaviour:

$$\langle v^4_{\rm LOS}\rangle = \begin{cases} A\left(\frac{R}{R_{\rm data}}\right)^{-\eta}, & R_{\rm data} < R < R_{\rm out}, \\ A\left(\frac{R_{\rm out}}{R_{\rm data}}\right)^{-\eta}\left(\frac{R}{R_{\rm out}}\right)^{-\kappa}, & R > R_{\rm out}, \end{cases} \tag{20}$$

where A and $-2 < \eta < 2$ are fitting parameters and $R_{\rm out}$ sets the outer 'edge' of the galaxy. We assume flat priors on $R_{\rm out}$ of $R_{\rm data} < R_{\rm out} < 2R_{\rm data}$, and on the fall-off of $\langle v^4_{\rm LOS}\rangle$ beyond $R_{\rm out}$ of $1 < \kappa < 3$. To determine errors on v_{s1} and v_{s2}, we fit the above power law to each of 1000 Monte Carlo draws of the error distribution of $\langle v^4_{\rm LOS}\rangle$, as in Read & Steger (2017), marginalizing over $R_{\rm out}$ and κ. In this way, if either v_{s1} or v_{s2} are sensitive to the (unmeasured) large R behaviour of $\langle v^4_{\rm LOS}\rangle$, then the errors on these quantities will simply grow. If the data are good enough, however, then the above marginalization will little affect v_{s1} and/or v_{s2}. In tests, we found that the above scheme produces less bias for mocks where $\langle v^4_{\rm LOS}\rangle$ is steeply rising at the outermost data point. We will demonstrate its performance on three tidally stripped mocks in Section 4.

GravSphere fits the above model to the surface density profile of tracer stars, $\Sigma_*(R)$, their line-of-sight projected velocity dispersion profile $\sigma_{\rm LOS}(R)$, and their VSPs using the EMCEE affine invariant Markov Chain Monte Carlo (MCMC) sampler from Foreman-Mackey et al. (2013). We assume uncorrelated Gaussian errors such that the Likelihood function is given by $\mathcal{L} = \exp(-\chi^2/2)$, where χ^2 includes the contributions from the fits to Σ_*, $\sigma_{\rm LOS,}$ and the two VSPs. We use as default 1000 walkers, each generating 5000 models and we throw out the first half of these as a conservative 'burn in' criteria. (See Read & Steger (2017) for further details of our methodology and priors.)

3.2 The SIDM model

In addition to GravSphere's default free-form mass model (Section 3.1), we also implement a mass model that describes dark

matter halos in an ΛSIDM cosmology. While more restrictive than our free-form model, this has the advantage that the model parameters correspond to cosmologically interesting quantities like the dark matter halo mass and the SIDM self-interaction cross-section. Following Dooley et al. (2016), Schneider et al. (2017), and Contenta et al. (2018), we consider a velocity-independent SIDM model with an interaction cross section given by:

$$\frac{\sigma}{m} = \frac{\sqrt{\pi}\,\Gamma}{4\rho_{\rm NFW}(x)\sigma_v(x)} \tag{21}$$

where Γ is the SIDM interaction rate, x is a normalization scale for Γ (of which more shortly), $\rho_{\rm NFW}(x)$ is the NFW dark matter density at x before SIDM core formation (equation (1)), and:

$$\sigma_v^2(x) = \frac{G}{\rho_{\rm NFW}}\int_x^\infty \frac{M_{\rm NFW}(r')\rho_{\rm NFW}(r')}{r'^2}dr' \tag{22}$$

is the velocity dispersion of the dark matter halo at x before SIDM core formation. (We assume in this model that the velocity distribution is isotropic.)

We use a coreNFW profile (equation (9)) with $n = 1$ to describe the radial density profile of halos in SIDM, as in Schneider et al. (2017). However, since we are interested here in satellite galaxies that may have had their outer dark matter density steepened by tidal stripping, we modify the coreNFW profile to account for this, obtaining a new 'coreNFWtides' model:

$$\rho_{\rm cNFWt}(r) = \begin{cases} \rho_{\rm cNFW}, & r < r_t, \\ \rho_{\rm cNFW}(r_t)\left(\frac{r}{r_t}\right)^{-\delta}, & r > r_t, \end{cases} \tag{23}$$

where $\rho_{\rm cNFW}$ is as in equation (9), r_t sets the radius at which mass is tidally stripped from the galaxy, and δ sets the logarithmic density slope beyond r_t.

The coreNFWtides model has a number of advantages over previous fitting functions used in the literature. First, it is fully analytic with cumulative mass given by:

$$M_{\rm cNFWt}(<r) = \begin{cases} M_{\rm cNFW}(<r), & r < r_t \\ M_{\rm cNFW}(r_t) + & \\ 4\pi\rho_{\rm cNFW}(r_t)\frac{r_t^3}{3-\delta}\left[\left(\frac{r}{r_t}\right)^{3-\delta} - 1\right], & r > r_t \end{cases} \tag{24}$$

where $M_{\rm cNFW}$ is as in equation (6). Secondly, it retains the physical meaning of M_{200} and c_{200} in the NFW profile (equation (1)), while introducing two new physically motivated parameters, r_t and δ, to model the effect of tidal stripping beyond r_t.

We calibrate the above SIDM model using the Vogelsberger, Zavala & Loeb (2012) pure dark matter cosmological zoom simulations of Milky Way-mass halos in an ΛSIDM cosmology. Our goal is to ensure that our SIDM model correctly recovers the density profile and scatter of the 15 most massive subhalos in these simulations, since these are the subhalos in which Draco is most likely to reside (Zavala, Vogelsberger & Walker 2013). Our free parameters in the calibration are the interaction rate, Γ, and its normalisation scale, x (see equation 21). Typically, x is taken to be the dark matter core size, $x \sim r_c$, for which the interaction rate required to produce a core on the scale of r_c in a Hubble time is of order unity, $\Gamma \sim 1\,{\rm Gyr}^{-1}$ (e.g. Vogelsberger et al. 2012; Dooley et al. 2016). However, in tests we found that, for our coreNFWtides model, using equation (21) with $x = r_c$ gives a poor fit to the density profiles of subhalos in the Vogelsberger et al. (2012) SIDM simulations for any choice of constant Γ. From inspection of equation (21), we can understand why this occurs. Notice that, for a constant σ/m, the density and dispersion at r_c will both fall as the SIDM core forms, lowering Γ. Since the rate at which this occurs depends on σ/m, there is no choice of constant Γ that can simultaneously fit simulations with low and high σ/m. We can, however, solve this problem by normalizing Γ instead at some larger radius $x \gg r_c$ at which the density profile and dispersion change very little after SIDM core formation. We find that $x = 10\,r_c$ with $\Gamma = 0.005\,{\rm Gyr}^{-1}$ gives a good fit to the density profiles of SIDM subhalos in the Vogelsberger et al. (2012) simulations.[2]

To demonstrate that our SIDM model provides a faithful reproduction of subhalos in the Vogelsberger et al. (2012) simulation, we perform 50 random draws of the 15 most massive subhalos from the subhalo distribution function described in[3] Springel et al. (2008). For each halo, we draw its concentration from the $M_{200} - c_{200}$ relation of Dutton & Macciò (2014), multiplied by a factor of 1.4 to account for the increased concentration of subhalos as compared to field halos (Springel et al. 2008), and allowing for a scatter of 0.1 dex. We then use our SIDM model, above, to calculate the radial density profile of each halo for a given choice of σ/m. Marginalizing over all drawn halos, we calculate the median radial density profiles for each σ/m and their 68 per cent confidence intervals. The results are shown in Fig. 2. The panels show the median density profiles (solid lines) and 1σ scatter (contours) for the 15 most massive SIDM subhalos in the Vogelsberger et al. (2012) SIDM simulations[4] (top) and from our SIDM model (bottom), calculated as described above. The black lines and contours show results for an ΛCDM cosmology, while the other coloured lines and bands show results for an ΛSIDM cosmology with an SIDM cross section of $\sigma/m = 0.1$, 1 and $10\,{\rm cm}^2/{\rm g}$, as marked. As can be seen, our SIDM model is in good agreement with the median density profile and scatter of subhalos in the Vogelsberger et al. (2012) simulations.

Note that our SIDM model is calibrated on one particular set of SIDM simulations. As such, it is not clear if it can be successfully extrapolated to velocity-dependent cross-sections, field halos, or halos with a very different mass to those studied here. Furthermore, the model does not include the effect of core collapse. Core collapse can occur for high cross-sections ($\sigma/m \gtrsim 10\,{\rm cm}^2/{\rm g}$), leading to a steep central density at late times (e.g. Balberg, Shapiro & Inagaki 2002; Vogelsberger et al. 2012). We discuss this further in Section 7. Finally, our model does not include the effect of the baryonic potential on the SIDM density profile (e.g. Kaplinghat et al. 2014; Robertson et al. 2018). This latter is not likely, however, to be a significant effect for Draco whose mass profile is dominated at all radii by dark matter (e.g. Kleyna et al. 2001).

When using the coreNFWtides model to describe SIDM halos, we fit the following free parameters: the halo mass and concentration before infall: M_{200} and c_{200}; the dark matter core-size parameter r_c; the tidal stripping radius r_t and the logarithmic density slope beyond r_t, δ. We assume flat priors of $8.75 < \log_{10}(M_{200}/{\rm M}_\odot) < 10.25$; $10 < c_{200} < 22$; $-2 < \log_{10}(r_c/{\rm kpc}) < 0.5$; $0.3 < \log_{10}(r_t/R_{1/2}) < 1$; and $3.5 < \delta < 5$ on these parameters. Our results are not sensitive to these choices. (In particular, extending the upper bound on c_{200} to be $c_{200} < 40$ to account for the higher concentration of subhalos

[2] In fact, it is the ratio $\Gamma/\rho_{\rm NFW}(x)$ that is important (see equation 21). Since at large x, $\rho_{\rm NFW} \propto x^{-3}$, we can find equivalently good fits for $x > 10\,r_c$ and $\Gamma = 0.005\,(10\,r_c/x)^{-3}\,{\rm Gyr}^{-1}$.

[3] The Vogelsberger et al. (2012) simulations are based on the Aquarius ΛCDM simulations described in Springel et al. (2008) and have, therefore, similar subhalo statistics (Zavala et al. 2013).

[4] This panel was adapted from a Figure in Zavala et al. (2013).

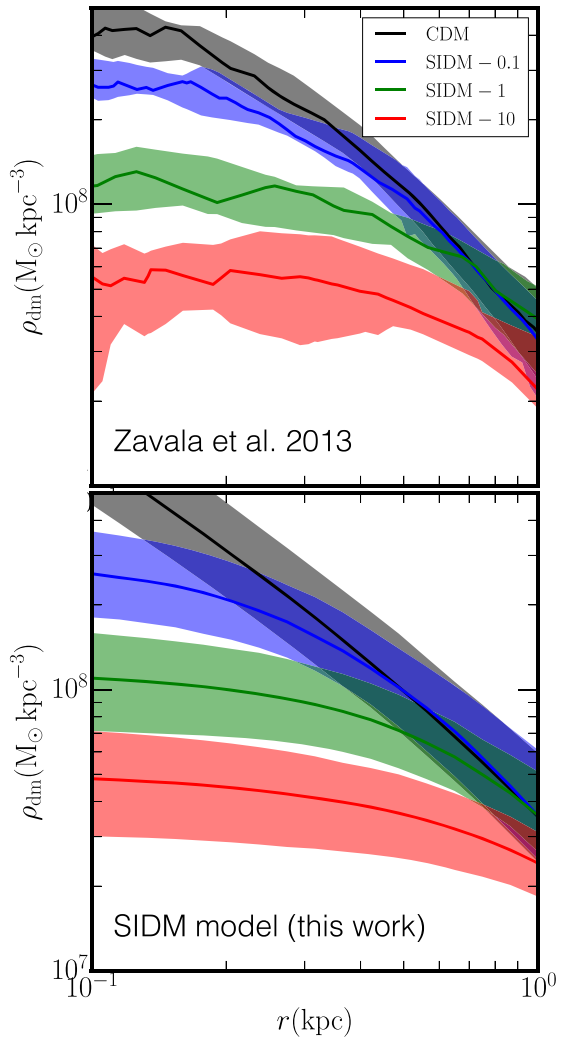

Figure 2. Calibrating our SIDM model. The panels show the median density profiles (solid lines) and 1σ scatter (contours) for the 15 most massive subhalos from the Vogelsberger et al. (2012) and Zavala et al. (2013) ΛSIDM simulations (top), and from our SIDM model (bottom; see text for details). The black lines and contours show results for a ΛCDM cosmology, while the other coloured lines and bands show results for a ΛSIDM cosmology with a SIDM cross section of $\sigma/m = 0.1$, 1 and 10 cm^2/g, as marked. As can be seen, our SIDM model is in good agreement with the median density profile and scatter of subhalos in the Vogelsberger et al. (2012) simulations.

in and ΛCDM (Springel et al. 2008, and see the discussion above) produces no appreciable effect on our results.)

4 TESTING GRAVSPHERE ON TIDALLY STRIPPED MOCK DATA

4.1 Three tidally stripped mock Dracos

GRAVSPHERE was extensively tested on mock data in Read & Steger (2017), including on triaxial mocks for which GRAVSPHERE (that assumes spherical symmetry) is expected to become biased. However, we did not test GRAVSPHERE on tidally stripped mock dwarfs. Such a test is relevant for our paper here since Draco orbits close to the Milky Way (see Section 1). We may worry, then, that tidal stripping will induce aspherical distortions and departures from equilibrium that could cause GRAVSPHERE to become biased (e.g. Kowalczyk et al. 2013). To test whether this is an issue for the GRAVSPHERE models, we present in this paper, three mocks, designed to mimic the Draco dwarf spheroidal galaxy as closely as possible: Mock–Cusp, Mock–Core and Mock–CoreDen, summarized in Table 1.

Table 1. Mock data initial conditions. From left to right, the columns give the mock data label, the CORENFW model parameters, the total simulation time, and the tidal stripping radius at pericentre, r_{tp} (calculated as in Read et al. (2006a) using the 'prograde' stripping radius; see text for details). The remaining model parameters for the mocks are identical. All three use the same double-Plummer light profile (equation 25), $N_{\rm DM} = 10^7$ dark matter and $N_* = 2 \times 10^7$ star particles, and force softenings $+_{\rm DM} = 0.009$ kpc and $+_* = 0.005$ kpc, respectively. The mocks were placed on the same orbit around the live Milky Way model from Read et al. (2008). See Section 4 for further details.

Label	CORENFW **parameters** $[M_{200}(\mathrm{M}_\odot), c_{200}, n, r_c(\mathrm{kpc})]$	$T_{\rm sim}$ [Gyrs]	$\mathbf{r_{tp}}$ [kpc]
Mock–Cusp	5×10^9, 14, 0, –	10	1.5
Mock–Core	5×10^9, 14, 1, 0.315	10	1.5
Mock–CoreDen	5×10^9, 35, 1, 0.315	4.16	2.3

The Mock–Cusp mock is designed to simulate a Draco with a 'pristine' dark matter cusp (see Section 1). The Mock–Core model is identical to the Mock–Cusp model, but with a constant density dark matter core of size $\sim R_{1/2}$. This core is consistent with complete core formation in the Read et al. (2016a) model, where the core owes to 'dark matter heating' due to bursty stellar feedback. It is also consistent with the SIDM model that we described in Section 3.2, corresponding to a self-interaction cross section of $\sigma/m = 0.22\,\mathrm{cm}^2/\mathrm{g}$. However, while the Mock–Core model is cosmologically realistic, its lower central density than the Mock–Cusp model makes it more susceptible to tidal stripping and shocking (e.g. Read et al. 2006a). For this reason, we include also the Mock–CoreDen model. This is substantially more concentrated than would be expected in either an ΛCDM or ΛSIDM cosmology, but may occur in other cosmological models. With the same initial density as the Mock–Cusp model at ∼50 pc, the Mock–CoreDen model allows us to test GRAVSPHERE on a cored mock that has experienced less tidal distortions than the Mock–Core model.

4.2 The stellar light profile and dark matter distribution

All three mocks were set up as a spherical galaxy with a double-Plummer sphere of stars:

$$\rho_* = \frac{3M_*}{8\pi}\left[\frac{1}{a_1^3}\left(1+\frac{r^2}{a_1^2}\right)^{-5/2} + \frac{1}{a_2^3}\left(1+\frac{r^2}{a_2^2}\right)^{-5/2}\right] \qquad (25)$$

with $M_* = 0.29 \times 10^6\,\mathrm{M}_\odot$, $a_1 = 0.12$ kpc and $a_2 = 0.23$ kpc.

This was embedded in a CORENFW dark matter halo profile (see Section 2). For the Mock–Cusp and Mock–Core mocks, we used $M_{200} = 5 \times 10^9\,\mathrm{M}_\odot$ and $c_{200} = 14$. For the Mock–CoreDen mock, we used $c_{200} = 35$. All three sampled the dark matter with $N_{\rm DM} = 10^7$ particles and the stars with $N_* = 2 \times 10^7$ particles. We used force softenings for the stars and dark matter of $+_* = 0.005$ kpc and $+_{\rm DM} = 0.009$ kpc, respectively. (We verified that our results are numerically converged at this resolution by comparing them with a similar simulation run with 1/10th of the number of particles. For a discussion of resolution requirements for tidal stripping simulations, we refer the reader to Kazantzidis et al. 2004, Read et al. 2006b and van den Bosch et al. 2018.)

For the Mock–Cusp model, we assumed a perfect NFW profile with $n = 0$ (a 'pristine' cusp). For the Mock–Core and Mock–

CoreDen models, we assumed maximal cores, with $n = 1$ and $r_c = 0.315$ kpc, corresponding to a visible core size (see Section 2) of $r_{cv} = R_{1/2}$.

4.3 The orbit and host Milky Way potential

The above mock dwarfs were placed on an orbit around a collisionless mock 'Milky Way', taken from Read et al. (2008). This Milky Way model had $N_* = 7.5 \times 10^5$ and $N_{\rm DM} = 2 \times 10^6$, with $+_* = 0.06$ kpc and $+_{\rm DM} = 0.1$ kpc. The stellar disc had mass and scale length $M_* = 3 \times 10^{10}$ M$_\odot$ and $r_* = 3$ kpc, respectively,[5] while its dark matter halo was also of NFW form, with $M_{200} = 10^{12}$ M$_\odot$ and an initial scale length, before growing the disc, of $r_s = 25$ kpc (after disc growth, the halo contracts yielding a scale length of $r_s \sim 12$ kpc). The mocks were placed on orbits consistent with Draco's recently measured proper motions (Sohn et al. 2017; Gaia Collaboration et al. 2018): $\mathbf{r}_i = [-4.3, 62.3, 43.3]$ kpc and $\mathbf{v}_i = [57.8, 18.2, -172.3]$ km/s in Galactocentric coordinates. This yields a peri- and apocentre of $r_p = 42$ kpc and $r_a = 123$ kpc, respectively, consistent with the orbit calculations in Sohn et al. (2017). The Mock-Cusp and Mock-Core models were evolved for 10 Gyrs using the PKDGRAV-2 N-body code (Stadel 2001). The Mock-CoreDen model was evolved for 4.16 Gyrs since longer evolution led to significant numerical relaxation inside $R_{1/2}$. The initial tidal radii of the mocks at pericentre, r_{tp}, are reported in Table 1. These were calculated as in Read et al. (2006a), assuming the 'prograde' stripping radius.[6]

In Fig. 3, we give a visual impression of the simulations used to produce our mock data. The plot shows the projected density of stars in the Mock–Cusp model. The stellar disc of the host 'Milky Way' is seen edge-on, while the dwarf is seen to the top right, as marked. Notice the prominent tidal tails produced as stars are tidally stripped from the mock dwarf by the 'Milky Way'. Such tidal stripping occurs in all three mocks, despite their initial tidal radii being substantially larger than their projected half-light radii (see Table 1). This occurs as tidal shocks slowly push stars and dark matter over the tidal boundary, gradually whittling the dwarf down (see e.g. Read et al. 2006a).

4.4 Binaries, foreground contamination and sampling

To generate our mock data for GRAVSPHERE, we attempt to mimic as closely as possible the true Draco data. First, we placed each mock Draco at a distance of $D = 82$ kpc. Next, we discarded all star particles at radii $R < 90$ arcmins (corresponding to 2.1 kpc at the distance of Draco). Then, we generated a foreground population of stars with uniform projected density within the $R < 90$ arcmin field of view. For this foreground population, we assumed ugriz photometry with radial velocities drawn from the Besançon model, as implemented in the `Galaxia` code (Robin et al. 2003; Sharma et al. 2011). We then kept only those foreground stars that pass the same isochrone-based filter that was applied to select real Draco targets (see Section 5). This provides us with a mock 'photometric' data set that represents a catalog of RGB candidates. We then sampled spectroscopic quantities for a subset of these mock RGB candidate stars, applying the position-dependent target selection corresponding to the real Draco selection described in Section 5. We scattered these individual stellar velocities according to errors drawn randomly from the real draco data (typically $\sim$1 km/s). We added binary components to 50 per cent of the member stars, corresponding to the fraction inferred from multi-epoch data for Draco by Spencer et al. (in preparation), using the distributions of binary orbital elements assumed in that work. Finally, we used the procedure described in Section 5 to obtain membership probabilities for the mock Draco stars. We sampled stars such that the final membership weighted number of mock Draco stars in the photometric and spectroscopic samples were $\sim$2000 and $\sim$500, respectively, similarly to the real Draco data (see Section 5). In Appendix B, we explore the effect of a larger spectroscopic sample size and the influence of binaries and foreground contamination on the Mock-Core mock. There, we show that the binaries and foreground contamination induce some bias in the recovered velocity anisotropy and density profile, but the effect is smaller than our 95 per cent confidence intervals. A larger spectroscopic sample size leads to tighter constraints on the density profile, as may be expected.

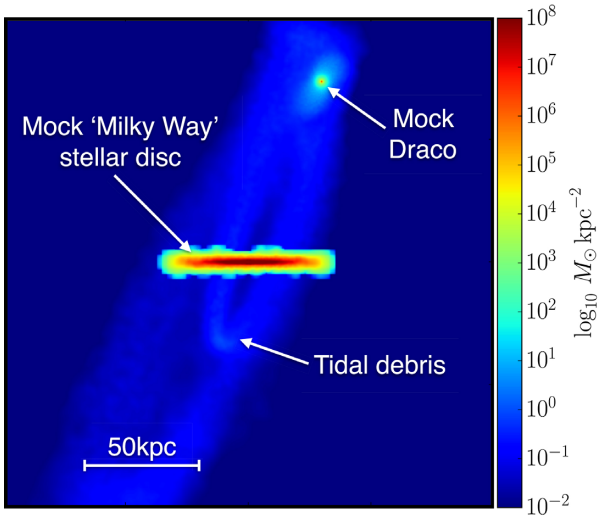

Figure 3. A visual impression of the simulations used to produce our mock data. The plot shows the projected density of stars in the Mock–Cusp model. The stellar disc of the host 'Milky Way' is seen edge-on, while the dwarf is seen to the top right, as marked. Notice the prominent tidal tails produced as stars are tidally stripped from the mock dwarf by the 'Milky Way'.

4.5 Results from applying GRAVSPHERE to the mock data

The GRAVSPHERE recovery for all three mocks is shown in Fig. 4. From left to right, the panels show the spherically averaged dark matter density profile, the logarithmic slope of the density profile ($\gamma_{\rm DM} = d\ln\rho/d\ln r$), and the symmetrised velocity anisotropy profile (equation (15)). The grey contours show the 68 per cent (dark grey) and 95 per cent (light grey) confidence intervals of the GRAVSPHERE models. The red lines in the left-hand panels show the dark matter density profile of the mocks prior to the action of tides. The blue lines in left-hand panels show the dark matter density profile

[5]The mass of this stellar disc is a factor $\sim$1.5 lower than that of the Milky Way (e.g. Bovy & Rix 2013). However, this is not likely to impact our results since neither the mock nor the real Draco comes closer than $\sim$40 kpc from the Galactic centre.

[6]Read et al. (2006a) show that stars moving prograde to the orbit of the satellite around the host galaxy are more easily stripped than stars moving on radial or retrograde orbits (see Holmberg (1941); Henon (1970); Keenan & Innanen (1975); D'Onghia et al. (2010) and Gajda & Łokas (2016) for earlier and later work on this effect). Over several orbits of the satellite around the host, Read et al. (2006a) find that stars near the tidal boundary of the satellite have their orbits transformed, leading to a gradual convergence towards the prograde stripping radius.

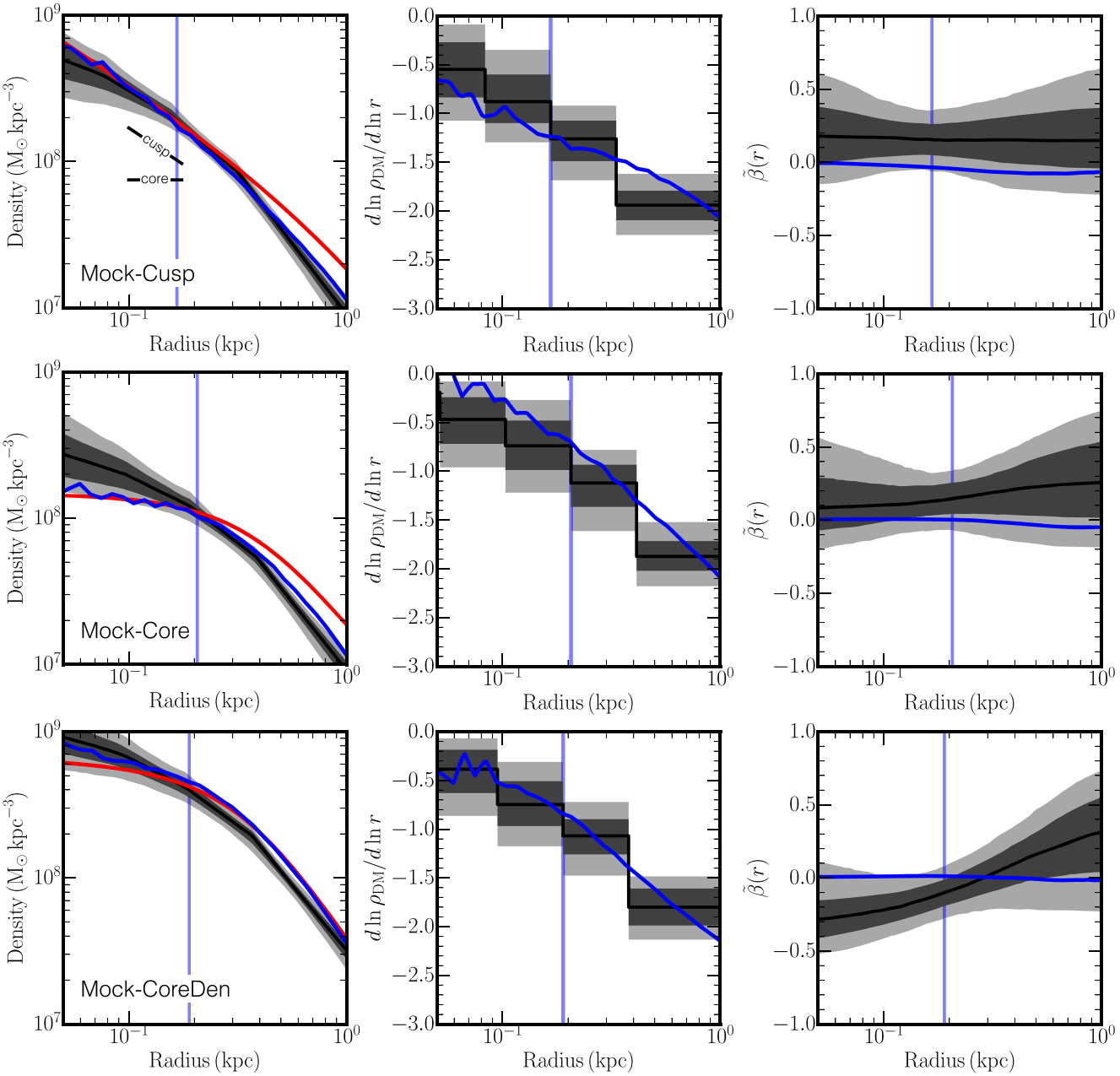

Figure 4. GRAVSPHERE recovery of the tidally stripped mock dwarfs. From top to bottom, the panels show results for the Mock–Cusp, Mock–Core and Mock–CoreDen mocks, as marked. From left to right, the panels show the spherically averaged dark matter density profile, the logarithmic slope of the density profile ($\gamma_{\rm DM} = d\ln\rho/d\ln r$), and the symmetrised velocity anisotropy profile (equation 15). The grey contours show the 68 per cent (dark grey) and 95 per cent (light grey) confidence intervals of the GRAVSPHERE models. The red lines in the left-hand panels show the dark matter density profile of the mocks prior to the action of tides. The blue lines in left-hand panels show the dark matter density profile after tidal stripping and shocking by a 'Milky Way'-like galaxy (see Section 4 for details). This is the 'correct answer' that GRAVSPHERE should recover. Similarly, the blue lines in the middle and right-hand panels show the correct $\gamma_{\rm DM}$ and velocity anisotropy profiles, respectively. In all panels, the vertical blue lines mark the projected half light radius of the stars, $R_{1/2}$.

after tidal stripping and shocking by a 'Milky Way'-like galaxy (see Section 4 for details). This is the 'correct answer' that GRAVSPHERE should recover. The blue lines in the middle and right-hand panels show, similarly, the correct $\gamma_{\rm DM}$ and velocity anisotropy profiles, respectively. In all panels, the vertical blue lines mark the projected half light radius of the stars, $R_{1/2}$. We show example fits to the data for the Mock–Core and Mock–Cusp mocks in Appendix A.

For the Mock–Cusp dwarf, GRAVSPHERE recovers the input density distribution within its 68 per cent confidence intervals (see Fig. 4, left-hand panel, top row). GRAVSPHERE correctly detects that this mock dwarf has a high central density of $\rho_{\rm DM}(150\,{\rm pc}) = 2.1^{+0.5}_{-0.4} \times 10^8\,{\rm M}_\odot\,{\rm kpc}^{-3}$ at 95 per cent confidence, consistent with a ΛCDM cusp (see Section 2), and that its outer density beyond $R_{1/2}$ has been steepened by tidal stripping. The logarithmic slope of the density profile, $\gamma_{\rm DM}(r)$, is recovered within GRAVSPHERE's 68 per cent confidence intervals (middle panel, top row); GRAVSPHERE finds $\gamma_{\rm DM}(150\,{\rm pc}) = -0.89^{+0.28}_{-0.25}$ as compared to the input model, $\gamma_{\rm DM,true}(150\,{\rm pc}) = -1.2$. There is, however, some weak ra-

dial bias in the symmetrised velocity anisotropy profile (right-hand panel, top row).

The Mock–Core dwarf is more challenging because of the larger effect of both tidal stripping and shocking. These cause the evolved dark matter density profile to separate from the input model at radii $R \gtrsim R_{1/2}$ (compare the blue and red lines in Fig. 4, left-hand panel, middle row). Nonetheless, GRAVSPHERE correctly recovers the input model within its 95 per cent confidence intervals. GRAVSPHERE correctly detects that this mock has a low central density of $\rho_{\rm DM}(150\,{\rm pc}) = 1.3^{+0.6}_{-0.7} \times 10^8\,{\rm M}_\odot\,{\rm kpc}^{-3}$ at 95 per cent confidence, consistent with a small dark matter 'core' within $R_{1/2}$ (see Section 2). The logarithmic slope of the density profile, $\gamma_{\rm DM}(r)$ (middle panel, middle row) is recovered within GRAVSPHERE's 68 per cent confidence intervals, but there is a small systematic bias towards cuspier models. GRAVSPHERE finds $\gamma_{\rm DM}(150\,{\rm pc}) = -0.72^{+0.27}_{-0.26}$ as compared to the input model, $\gamma_{\rm DM,true}(150\,{\rm pc}) = -0.54$. In tests, we found that this bias is present in 100 random realizations of the Mock–Core mock and so does not owe to an unfortunate random draw. Instead, the bias owes to our choice of priors on $\gamma_{\rm DM}$. We will explore this further in Section 4.6.

Finally, the Mock–CoreDen model presents a challenge not because of tides (it is almost completely immune to tidal effects due to its high density), but because its $\sigma_{\rm LOS}$ and $\langle v^4_{\rm LOS}\rangle$ rise steeply to large radii making it more challenging to obtain an unbiased estimate of v_{s2} (see Section 3). For this reason, there is some bias in the recovery of the density profile for this mock (bottom left-hand panel), though the effect is small. The logarithmic slope of the density profile, $\gamma_{\rm DM}$ (Fig. 4, middle panel, bottom row), is recovered within the 68 per cent confidence intervals of the GRAVSPHERE model chains. GRAVSPHERE finds $\gamma_{\rm DM}(150\,{\rm pc}) = -0.75^{+0.24}_{-0.22}$ as compared to the input model, $\gamma_{\rm DM,true}(150\,{\rm pc}) = -0.69$. The symmetrized velocity anisotropy (Fig. 4, right-hand panel, bottom row) is slightly biased towards tangential models at the centre and radial models at large radii.

4.6 The effect of our priors on $\gamma_{\rm DM}$

In this section, we explore the sensitivity of our results to our choice of priors on $\gamma_{\rm DM}$. Our default priors constrain $\gamma_{\rm DM}$ to lie in the range $-3 < \gamma_{\rm DM} < 0$ for each mass bin (see Section 3). In the absence of sufficiently constraining data, this could cause GRAVSPHERE to disfavour cores ($\gamma_{\rm DM} = 0$) because they occupy a smaller hypervolume of the solution space than cusps ($\gamma_{\rm DM} = -1$). To test this, we introduce a rather extreme prior on $\gamma_{\rm DM}$ designed to bias us towards cored models. We assume a flat prior over the range $-3 < \gamma'_{\rm DM} < 2$, and set $\gamma_{\rm DM} = 0$ if $\gamma'_{\rm DM} > 0$ and $\gamma_{\rm DM} = \gamma'_{\rm DM}$ otherwise. In the absence of constraining data, this biases GRAVSPHERE towards cores by creating a large region of hypervolume in which $\gamma_{\rm DM} = 0$. Note that we consider this prior to be extreme and use it only to test our sensitivity to priors on $\gamma_{\rm DM}$.

In Fig. 5, we rerun the Mock–Cusp (top) and Mock–Core (bottom) mocks using the above modified prior on $\gamma_{\rm DM}$. Notice that our inference of $\gamma_{\rm DM}(r)$ is affected by our choice of prior, with the Mock–Cusp mock now being biased towards cored models (top right-hand panel), while the Mock–Core mock is no longer biased (bottom right-hand panel). However, our inference of the amplitude of the inner density at 150 pc is unaffected by this change in the priors. We obtain $\rho_{\rm DM}(150\,{\rm pc}) = 1.3^{+0.4}_{-0.4} \times 10^8\,{\rm M}_\odot\,{\rm kpc}^{-3}$ at 95 per cent confidence for the Mock-Core mock and $\rho_{\rm DM}(150\,{\rm pc}) = 2.1^{+0.5}_{-0.4} \times 10^8\,{\rm M}_\odot\,{\rm kpc}^{-3}$ at 95 per cent confidence for the Mock-Cusp mock, consistent with our default prior estimates. Furthermore, in all cases – independently of our choice of prior – we recover $\rho_{\rm DM}(r)$ and $\gamma_{\rm DM}(r)$ within our 95 per cent confidence intervals. In Appendix B, we show that this sensitivity of $\gamma_{\rm DM}$ to our choice of priors diminishes with improved spectroscopic sampling and, therefore, improved constraints on the inner density profile. Finally, note that for 500 stars with spectroscopic velocities the bias on $\gamma_{\rm DM}(R < R_{1/2})$ due to our choice of priors is small, shifting our results by of order the size of our 68 per cent confidence intervals, even for this rather extreme choice of prior (compare the middle panels in Fig. 4 with the right-hand panels in Fig. 5). We will discuss this further when presenting our results for Draco in Section 6.

4.7 Testing the recovery of SIDM model parameters using mock data

In this section, we test whether GRAVSPHERE is able to correctly recover the SIDM model parameters from our Mock–Core and Mock–Cusp mocks. For this test, we apply GRAVSPHERE to the mock data, but using the SIDM mass model described in Section 3.2 rather than GRAVSPHERE's default free-form mass model (Section 3.1). The results are shown in Fig. 6. The left-hand panels show the marginalized histograms of the core size parameter, r_c, in the CORENFWTIDES model (equation 23). The right-hand panels show the same for the SIDM self-interaction cross section, σ/m. For the Mock–Cusp mock (top panels), the correct answer is $r_c = \sigma/m = 0$, while for the Mock–Core model, it is $r_c = 0.315$ kpc and $\sigma/m = 0.22\,{\rm cm}^2/{\rm g}$, as marked by the vertical blue lines. Notice than in both cases, r_c and σ/m are well-recovered. For the Mock–Cusp mock, this translates into upper bounds on both parameters, since a small core inside $\sim 0.5R_{1/2}$ is still permitted within the uncertainties. For the Mock–Core mock, GRAVSPHERE well-recovers r_c, though there is a weak tail to low r_c cuspy models. This translates into a second peak at low σ/m (bottom right-hand panel of Fig. 6).

5 DATA

As GRAVSPHERE fits both surface density and projected velocity dispersion profiles, we require both photometric and kinematic data that sample Draco's stellar population. For the photometric data we use the Pan-STARRS DR1 catalog (Flewelling et al. 2016), initially selecting point-like sources[7] within 1.5° of Draco's nominal centre at $\alpha_{\rm J2000} = 17{:}\,20{:}\,14.4$, $\delta_{\rm J2000} = +57{:}\,54{:}\,54$ (Martin, de Jong & Rix 2008). From these point sources we obtain a sample of candidate red giant branch (RGB) stars within Draco by selecting only sources that are brighter than $i \leq 21$ mag and deviate in colour-magnitude ($g - r$, i) space by less than + magnitudes from an old (age = 12 Gyr), metal-poor ([Fe/H] = −2.5) model isochrone (Dotter et al. 2008) that we shift by distance modulus $m - M = 19.6$, corresponding to Draco's distance of $D \sim 76$ kpc (McConnachie 2012). For this work, we adopt $\epsilon = \sqrt{0.04 + \sigma_i^2 + \sigma_{g-r}^2}$, where σ_i and σ_{g-r} are the Pan-STARRS uncertainties in magnitude and colour, respectively. This procedure yields a sample of 15,891 RGB candidates with uniform selection out to radius $R \leq 1.5°$.

For the stellar-kinematic data we adopt the spectroscopic sample published by Walker, Olszewski & Mateo (2015b), which consists of line-of-sight velocities, effective temperatures, surface gravities and metallicities measured for 1,565 RGB and horizontal branch

[7]We select point source objects for which the difference between PSF and Kron magnitudes in the r band is $r_{\rm PSF} - r_{\rm kron} < 0.05$ (see Farrow et al. 2014 for a discussion of Pan-STARRS star-galaxy separation).

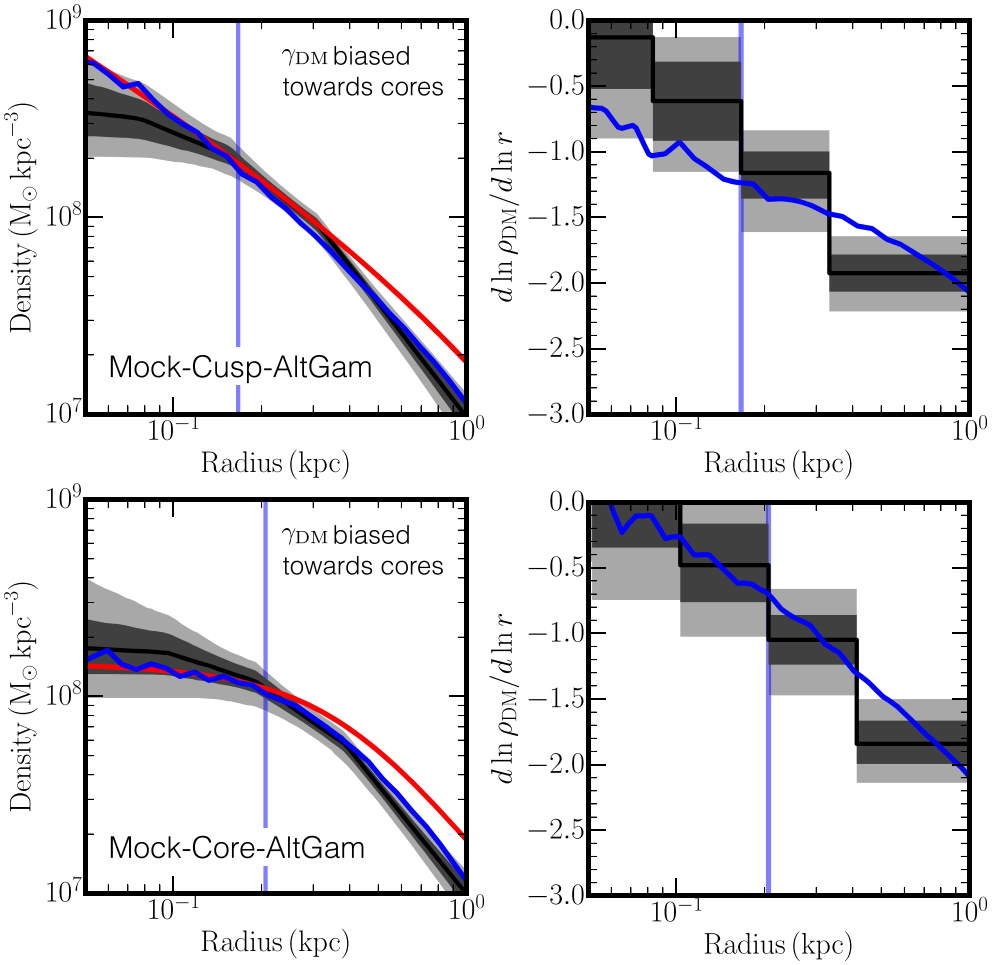

Figure 5. Testing the effect of our priors on $\gamma_{\rm DM}$. The plots show the dark matter density profile (left) and logarithmic density slope (right) of GravSphere models for the Mock–Cusp (top) and Mock–Core (bottom) mocks, but using a rather extreme prior on $\gamma_{\rm DM}$ that biases us towards cores (see text for details). The lines and contours are as in Fig. 4. Notice that our inference of $\gamma_{\rm DM}(r)$ (right-hand panels) is affected by our choice of prior, with the Mock–Cusp mock now being biased towards core models, while the Mock–Core mock is no longer biased (compare these results with those in the middle panels of Fig. 4). However, our inference of the amplitude of the inner density at 150 pc is unaffected by this change in the priors. We obtain $\rho_{\rm DM}(150\,{\rm pc}) = 1.3^{+0.4}_{-0.4} \times 10^8\,{\rm M}_\odot\,{\rm kpc}^{-3}$ at 95 per cent confidence for the Mock-Core mock and $\rho_{\rm DM}(150\,{\rm pc}) = 2.1^{+0.5}_{-0.4} \times 10^8\,{\rm M}_\odot\,{\rm kpc}^{-3}$ at 95 per cent confidence for the Mock–Cusp mock, consistent with our default prior estimates.

candidates within 1.5° of Draco's center. Applying hard cuts to separate members from foreground contamination according to each of these observables, Walker et al. (2015b) estimate that this sample contains ∼500 probable members of Draco.

In order to achieve a more quantitative separation between Draco members and contamination from the Galactic foreground, we fit an initial, chemodynamical mixture model similar to the one described in detail by Caldwell et al. (2017) for their analysis of the dwarf galaxy Crater 2. That is, we fit simultaneously for: 1) the position distribution of RGB candidates in the photometric sample; and 2) the joint distribution of velocities and metallicities of RGB candidates in the spectroscopic sample. Following Caldwell et al. (2017), this initial fit assumes that: 1) the positions of Draco members follow a (single-component) Plummer profile, with projected stellar density $\Sigma_{\rm Dra}(R) = L(\pi a^2)^{-1}(1 + R^2/a^2)^{-2}$, where L and a are Draco's total luminosity and projected half-light radius, respectively; 2) the velocities, V, and metallicities, Z, of Draco members follow independent normal distributions: $P_{\rm Dra}(V, Z) = \mathcal{N}(\overline{V}, \sigma_V^2 + \delta_V^2)\mathcal{N}(\overline{Z}, \sigma_Z^2 + \delta_Z^2)$, where $\overline{V}$ and $\overline{Z}$ are mean velocity and mean metallicity, σ_Z and σ_Z are intrinsic velocity and metallicity dispersions, and δ_V, δ_Z are observational errors; 3) non-members in the Galactic foreground follow a uniform spatial distribution, $\Sigma_{\rm MW}$ = constant, with velocity and metallicity distributions estimated empirically by smoothing the data with a Gaussian kernel, denoting these estimates $\hat{P}_{\rm MW}(V)$ and $\hat{P}_{\rm MW}(Z)$. Our initial model is simpler than that of Caldwell et al. (2017), however, in that we assume that any velocity and/or metallicity gradients are negligible. After fitting this model, we evaluate for every star a probability of Draco membership,[8] $P_{\rm mem}(R, V, Z) = M/(M + N)$, where $M \equiv \Sigma_{\rm Dra}(R)P_{\rm Dra}(V, Z)$ and $N \equiv \Sigma_{\rm MW}(R)\hat{P}_{\rm MW}(V)\hat{P}_{\rm MW}(Z)$. Summing these probabilities, we estimate that the photometric sample of RGB candidates contains $N_{\rm mem,phot} = \sum_{i=1}^{N_{\rm phot}} P_{\rm mem,phot,i} =$

[8]The majority of stars in the photometric sample lack spectroscopic velocity and metallicity measurements; for these stars we evaluate membership probability using a simplified model wherein the probabilities of spectroscopically-observed quantities are set equal to unity and the membership probability depends solely on position.

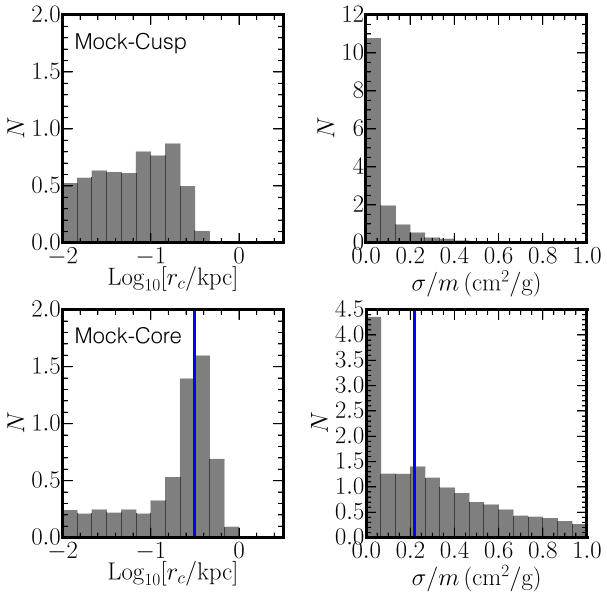

Figure 6. Testing the recovery of the SIDM model parameters using the Mock-Cusp (top) and Mock-Core (bottom) mocks. The left-hand panels show the marginalized histograms of the core-size parameter, r_c, in the coreNFWtides model (equation (23)). The right-hand panels show the same for the SIDM self-interaction cross section, σ/m. For the Mock-Cusp mock (top panels), the correct answer is $r_c = \sigma/m = 0$, while for the Mock–Core model, it is $r_c = 0.315$ kpc and $\sigma/m = 0.22\,\mathrm{cm}^2/\mathrm{g}$, as marked by the vertical blue lines.

$2,500 \pm 56$ members of Draco, while the spectroscopic one contains $N_{\rm mem,spec} = \sum_{i=1}^{N_{\rm spec}} P_{\rm mem,spec,i} = 504 \pm 1$ members.

We construct empirical surface density and projected velocity dispersion profiles for Draco by dividing the photometric and spectroscopic data sets, respectively, according to projected radius into annular bins. Each of these bins contains an equal membership-probability-weighted number of stars. We adopt $N_{\rm phot} = N_{\rm kin} = 15$ for both the surface density profile and the velocity dispersion profile. Fig. A1 displays the stellar surface density and projected velocity dispersion profiles that we obtain for Draco.

This construction of the binned profiles is imperfect for several reasons. First, the profiles reflect only the median posterior probability of membership for each star, and thus do not propagate variance in those membership probabilities. Second, the membership probabilities are derived from a model that incorporates simplifying assumptions—e.g. that the stellar positions follow a single-component Plummer profile and that the velocities follow a single Gaussian distribution—that are generally inconsistent with the one that GravSphere subsequently fits. A fully consistent treatment would require allowing for position-dependent and/or non-Gaussian velocity distributions and building a background model into our GravSphere analysis, a task that we reserve for future work. For now, we have confirmed that our results for Draco are qualitatively unchanged if we use for the initial fit a more sophisticated model that is based on the spherical Jeans equation, explicitly includes a dark matter halo and thereby allows the stellar velocity dispersion (and resulting dependence of membership probability on velocity) to vary with radius. For details of this model, see Section 4.5 of Caldwell et al. (2017).

Finally, Jardel et al. (2013) obtained a measurement of the inner dispersion profile of Draco at ∼5 pc from its centre using Virus-P spectrograph velocity measurements for 17 stars, of which 12 were found to be members of Draco. We experimented with including also these data, however they led to no noticeable change in our favoured distribution of models for Draco. As such, we present here results only using the Walker et al. (2015a) data that are selected and reduced in a fully consistent manner, with a consistent membership criteria.

6 RESULTS FOR DRACO

6.1 The dark matter density profile

In this section, we apply GravSphere to the real Draco data from Walker et al. (2015a) (see Section 5). The results are shown in Fig. 7, where the lines and panels are as in Fig. 4. (We show the GravSphere fits to the projected velocity dispersion, photometric light profile and VSPs in Appendix A, Fig. A.)

First, notice that – as for our mock data – we obtain strong constraints on $\tilde{\beta}$ only near the projected half stellar mass radius, $R_{1/2}$ (vertical blue line). The GravSphere models for Draco are consistent with velocity isotropy at all radii, similarly to our mock data.

The key result for this paper is the spherically averaged dark matter density profile for Draco (Fig. 7, left-hand panel). Marked on this panel are a power law cusp and a core. As can be seen, our GravSphere models for Draco are more similar to the cusped model, with a large central density, $\rho_{\rm DM}(150\,{\rm pc}) = 2.4^{+0.5}_{-0.6} \times 10^8\,{\rm M}_\odot\,{\rm kpc}^{-3}$ and logarithmic slope $\gamma_{\rm DM}(150\,{\rm pc}) = -0.95^{+0.50}_{-0.46}$ at 95 per cent confidence. In Appendix C, we show that this high central density is robust to modelling Draco without v_{s1} or v_{s2} (equations 17 and 19), and to changing the priors on $\gamma_{\rm DM}$. Switching to a rather extreme prior that biases us towards cored models (see Section 4.6), we find $\rho_{\rm DM}(150\,{\rm pc}) = 2.1^{+0.5}_{-0.6} \times 10^8\,{\rm M}_\odot\,{\rm kpc}^{-3}$, with a logarithmic slope of $\gamma_{\rm DM}(150\,{\rm pc}) = -0.7^{+0.52}_{-0.52}$ at 95 per cent confidence that still favours a cusp.

Our GravSphere models for Draco are in good agreement with pure dark matter structure formation simulations in ΛCDM (e.g. Dubinski & Carlberg 1991; Navarro et al. 1996b; and Section 1). We consider, next, what such a steep cusp in Draco implies for self-interacting dark matter models.

6.2 A new constraint on the self-interacting dark matter (SIDM) cross-section

In this section, we fit the SIDM model described in Section 3.2 to the data for Draco to place a new upper bound on the SIDM cross section. The results are shown in Fig. 8. The left-hand panel shows the marginalised histogram of dark matter core-size parameters, r_c (equation 23); the right-hand panel shows the corresponding histogram of SIDM self-interaction cross sections, σ/m, for this same model. Notice that models with large dark matter cores are disfavoured. We find, subject to our choice of SIDM model and prior, $r_c < 0.36$ kpc at 99 per cent confidence, corresponding to a visible core size of $r_{cv} < 0.21$ kpc at 99 per cent confidence (see Section 4). Thus, consistent with our free-form models for Draco, our SIDM models imply that, if Draco has a dark matter core, it is likely smaller than $R_{1/2}$. This upper bound on r_c corresponds to a new constraint on the SIDM self-interaction cross-section of $\sigma/m < 0.32\,\mathrm{cm}^2/\mathrm{g}$ at 95 per cent confidence and $\sigma/m < 0.57\,\mathrm{cm}^2/\mathrm{g}$ at 99 per cent confidence. (Recall that the mapping between r_c and σ/m depends also on the halo mass and concentration.)

For the other coreNFWtides parameters, we obtain a constraint on the pre-infall halo mass of Draco of $M_{200} = 2.6^{+1.1}_{-0.8} \times 10^9\,{\rm M}_\odot$

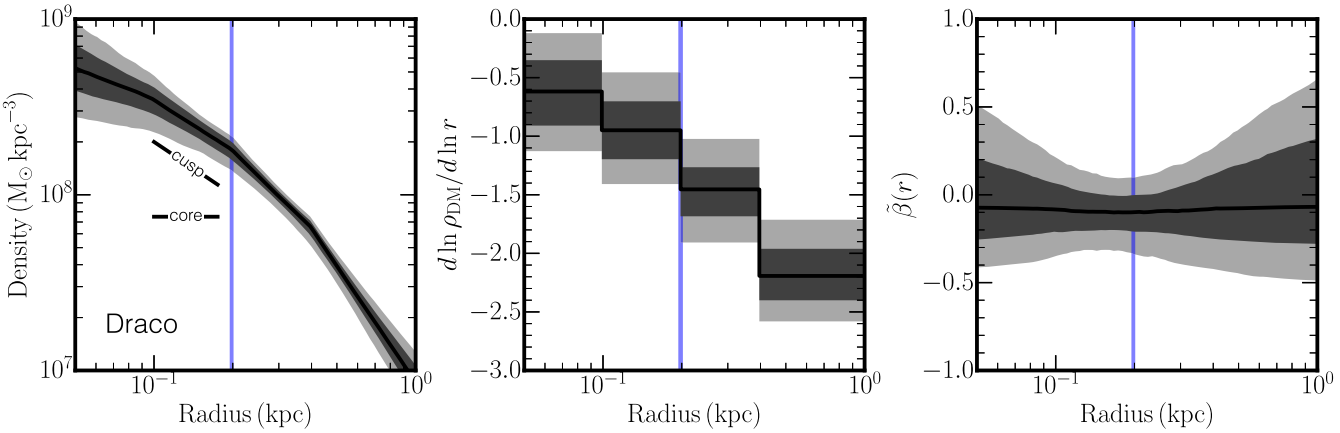

Figure 7. As Fig. 4, but for the real Draco data.

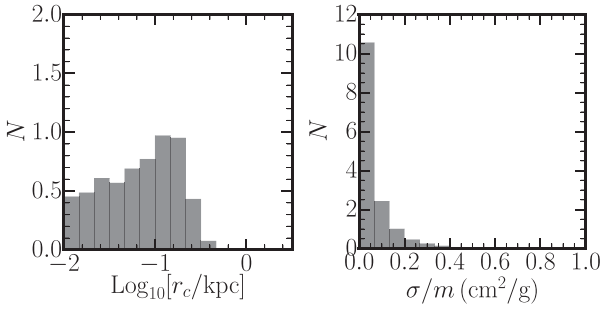

Figure 8. A new constraint on the SIDM self-interaction cross-section. The left-hand panel shows the marginalised histogram of dark matter core-size parameters, r_c, from fitting the SIDM CORENFWTIDES model to the Draco data (equation 23). The right-hand panel shows the corresponding histogram of SIDM self-interaction cross sections σ/m for this same model. The high central density that we infer for Draco disfavours models with $\sigma/m > 0.57\,\mathrm{cm}^2/\mathrm{g}$ at 99 per cent confidence.

at 68 per cent confidence, consistent with our mock Draco models (Section 4). We do not obtain strong constraints on c_{200}, δ nor r_t (see equation ((23)) for a definition of these).

7 DISCUSSION

7.1 Model caveats

There are three main caveats to our result that Draco has a central dark matter cusp. First, GRAVSPHERE, while being largely assumption-free, still assumes spherical symmetry and dynamic equilibrium. In Read & Steger (2017), we tested GRAVSPHERE on triaxial mock data that had triaxiality of the magnitude expected in ΛCDM. We found that the systematic error that this induces is typically smaller than the 95 per cent confidence intervals of the GRAVSPHERE models. Furthermore, when the systematic bias did become significant, the model fit was poor. We see no evidence of this behaviour for Draco (Fig. A1). This is consistent with other work in the literature that has found that spherical models can successfully recover the radial density profile of triaxial mock data (Laporte, Walker & Peñarrubia 2013; Genina et al. 2018; Kowalczyk, Lokas & Valluri 2018). In Section 4, we showed further that tidally stripped stars in Draco are also unlikely to influence our result. This is in tension with previous findings by Kowalczyk et al. (2013) who report a significant bias when applying spherical equilibrium models to tidally stripped mocks. This difference could owe to the fact that Kowalczyk et al. (2013) test simple Jeans mass estimators that are known to be more biased than fully self-consistent dynamical models (e.g. Campbell et al. 2017), or it could owe to their tidally stripped mocks being much further from equilibrium than the Mock–Cusp, Mock–Core, and Mock–CoreDen models that we consider here. It is beyond the scope of this present work to explore this in more detail.

The second potential caveat to our results is in our choice of data selection and binning. To test the importance of this, we ran a large suite of GRAVSPHERE models for Draco varying the data binning and membership selection criteria (see Section 5). In all cases, we found a central cusp, consistent with that in Fig. 7 (left-hand panel). However, it could be that our assumption of a Gaussian velocity distribution function when calculating the membership probability could bias our results, particularly at large radii where contamination is more problematic (see Section 5). We will explore this further in future work.

Finally, in Section 4 we found that with only 500 stars with spectroscopic data, GRAVSPHERE was able to distinguish $\rho_{\rm DM}(150\,\mathrm{pc})$ for our Mock-Cusp and Mock-Core mocks at 95 per cent confidence. However, the logarithmic slope of the density profile, $\gamma_{\rm DM}(150\,\mathrm{pc})$, depended on our choice of prior. Using a more conservative prior on $\gamma_{\rm DM}$ that is biased towards cores, we found $\gamma_{\rm DM} < -0.2$ at 95 per cent confidence, providing only weak evidence for a formal cusp. Increasing the spectroscopic sampling for Draco to 1000−2000 stars would reduce our sensitivity to the priors on $\gamma_{\rm DM}$ and improve our constraints (see Appendix B).

7.2 Comparison with previous work

Draco has long been known to be one of the densest of the Milky Way dwarfs (e.g. Kleyna et al. 2001). For this reason, it consistently features high on the list of targets for dark matter annihilation and decay searches (e.g. Charbonnier et al. 2011; Bonnivard et al. 2015; Evans, Sanders & Geringer-Sameth 2016). However, only one study to date has reported being able to constrain the central logarithmic slope of Draco's dark matter profile. Jardel et al. (2013) used a non-parametric Schwarzschild method applied to stellar kinematic data near the centre of Draco, obtained with the Virus-P spectrograph. They found a central logarithmic cusp slope

of $\gamma_{\rm DM} = -1.0 \pm 0.2$ over the range $20 < r < 700$ pc. This agrees well with our GravSphere models for Draco. More recently, Valli & Yu (2017) fit SIDM models to Draco, finding that Draco favours a low $\sigma/m \lesssim 0.5\,{\rm cm}^2/{\rm g}$, consistent with our findings here. This latter study is particularly interesting. They fit all of the Milky Way classical dwarfs with an SIDM model, finding a range of central densities that translates into a broad range of favoured σ/m. We will discuss this further in a companion paper where we apply GravSphere to all of the Milky Way classical dwarfs.

7.3 A small dark matter core in Draco

We have shown that our GravSphere models for Draco favour a dark matter cusp over the range $100 < R/{\rm pc} < R_{1/2}$. However, this still leaves room for a $\lesssim 100$ pc dark matter core within our GravSphere model uncertainties (Fig. 7, left-hand panel). This is interesting for two reasons. First, our SIDM model constraints are based on a velocity-independent SIDM model fit to a particular set of SIDM simulations (Section 3.2). As has been pointed out by several authors, SIDM can have a rather rich and complex dynamics due to, for example, late-time core collapse and tidal effects (e.g. Balberg et al. 2002; Vogelsberger et al. 2012). It could be that more detailed SIDM models have smaller central cores that are able to match the data for Draco with larger cross sections than we report here. Secondly, two studies have recently used the survival and properties of dense star clusters in the 'ultra-faint' dwarfs Eridanus II (Amorisco 2017; Contenta et al. 2018) and Andromeda XXV (Amorisco 2017) to argue for the presence of dark matter cores. This raises an important question: are the claimed dark matter cores in Eridanus II and Andromeda XXV at odds with our findings here for Draco?

First, note that Contenta et al. (2018) show that Eridanus II's dark matter core has a size >45 pc and a density in the range $6 \times 10^7 - 2.5 \times 10^8\,{\rm M}_\odot\,{\rm kpc}^{-3}$. Draco could host a $\lesssim 100$ pc-size dark matter core at the upper end of this range (see Fig. 7, left-hand panel). Such a core could result from a modification to dark matter (e.g. SIDM with a low self-interaction cross section). However, it seems unlikely that this same model could then be responsible also for the much larger dark matter core reported in Fornax (e.g. Goerdt et al. 2006; Walker & Peñarrubia 2011; Cole et al. 2012; Pascale et al. 2018) and the similarly large cores reported in nearby gas-rich isolated dwarf irregulars (e.g. Moore 1994; Flores & Primack 1994; Read et al. 2017). By contrast, models in which dark matter is heated by bursty stellar feedback could naturally account for such a diversity of central dark matter densities, at least in principle. Recall that whether or not a dark matter core can form from such 'heating' depends on: (i) the pre-infall dark matter halo mass, M_{200}; (ii) the halo concentration parameter, c_{200}; (iii) the total stellar mass, M_*; and (iv) the size of the dark matter core (e.g. Di Cintio et al. 2014; Read et al. 2016a; Contenta et al. 2018; Bermejo-Climent et al. 2018). (Smaller cores require less energy to form and form more rapidly.) Dark matter cores are also easier to form at high redshift when the star formation rates are high and the halo masses are smaller (Madau, Shen & Governato 2014). This suggests that *small* ($\lesssim 100$pc) dark matter cores may indeed form very early in the Universe even in ultra-faint dwarfs. This effect could be ubiquitous, or it could be stochastic, depending on the merger history, spin and/or concentration of any given dwarf (e.g. Laporte & Peñarrubia 2015). We will return to this issue in more detail in a forthcoming paper where we present GravSphere models for all of the Milky Way classical dwarfs.

8 CONCLUSIONS

We have used a new mass modelling method, GravSphere, to measure the central dark matter density profile of the Draco dwarf spheroidal galaxy. Our key findings are as follows:

(i) Using mock data with sampling, binary star population, and foreground contamination similar to that for the real Draco dwarf, we showed that GravSphere is able to successfully recover the dark matter density profile of a tidally stripped Draco-like dwarf within its 95 per cent confidence intervals (Fig. 4). However, while we were able to distinguish the amplitude of the central density, $\rho_{\rm DM}(150\,{\rm pc})$, of our cored and cusped mocks at 95 per cent confidence, the logarithmic slope of the density profile, $\gamma_{\rm DM}(150\,{\rm pc})$, depended on our choice of priors. This sensitivity to the prior diminishes with improved spectroscopic sampling (Appendix B).

(ii) We then applied GravSphere to the real Draco data. We inferred a high central density of $\rho_{\rm DM}(150\,{\rm pc}) = 2.4^{+0.5}_{-0.6} \times 10^8\,{\rm M}_\odot\,{\rm kpc}^{-3}$ with logarithmic slope $\gamma_{\rm DM}(150\,{\rm pc}) = -0.95^{+0.50}_{-0.46}$ at 95 per cent confidence, consistent with expectations from pure-dark matter structure formation simulations in ΛCDM (Fig. 7). We tested the robustness of this result, showing that even using a rather extreme prior on $\gamma_{\rm DM}$ that biases us towards cored models, our GravSphere models still favour a logarithmic slope of $\gamma_{\rm DM}(150\,{\rm pc}) = -0.70^{+0.52}_{-0.52}$ at 95 per cent confidence, steeper than that of a uniform-density core. Dark matter models with a high central density and a shallow inner slope are, however, still permitted.

(iii) At smaller radii, $R < 0.5R_{1/2}$, our GravSphere model constraints are poorer, consistent with both a dark matter cusp and a core within our 95 per cent confidence intervals.

(iv) We fit a velocity-independent SIDM model to the Draco data, obtaining – subject to our choice of SIDM model and prior – a new upper bound on the dark matter self-interaction cross section of $\sigma/m < 0.32\,{\rm cm}^2/{\rm g}$ at 95 per cent confidence and $\sigma/m < 0.57\,{\rm cm}^2/{\rm g}$ at 99 per cent confidence. This illustrates how Draco's high central density, in combination with constraints on the density profile at larger radii, can be used to constrain interesting dark matter models. We will consider in future work whether such a high density can be consistent with other modifications to dark matter.

(v) Finally, our SIDM model fit also provided a constraint on the pre-infall dark matter halo mass of Draco. We found $M_{200} = 2.6^{+1.1}_{-0.7} \times 10^9\,{\rm M}_\odot$ at 68 per cent confidence.

ACKNOWLEDGEMENTS

We would like to thank Manoj Kaplinghat, Giuseppina Battaglia, Aurel Schneider, Richard Massey, Andrew Robertson, and the anonymous referee for helpful feedback on an early draft of this paper. JIR would like to thank the KITP in Santa Barbara and the organisers of the 'The Small-Scale Structure of Cold(?) Dark Matter' programme. This paper benefited from helpful discussions that were had during that meeting. JIR would like to acknowledge support from SNF grant PP00P2_128540/1, STFC consolidated grant ST/M000990/1 and the MERAC foundation. This research was supported in part by the National Science Foundation under Grant No. NSF PHY-1748958. M.G.W. is supported by National Science Foundation grant AST-1412999. Fig. 3 and the mock data analysis made use of the excellent `PyNbody` software package[9] (Pontzen et al. 2013).

[9] https://github.com/pynbody/pynbody.

The Pan-STARRS1 Surveys (PS1) and the PS1 public science archive have been made possible through contributions by the Institute for Astronomy, the University of Hawaii, the Pan-STARRS Project Office, the Max-Planck Society and its participating institutes, the Max Planck Institute for Astronomy, Heidelberg and the Max Planck Institute for Extraterrestrial Physics, Garching, The Johns Hopkins University, Durham University, the University of Edinburgh, the Queen's University Belfast, the Harvard-Smithsonian Center for Astrophysics, the Las Cumbres Observatory Global Telescope Network Incorporated, the National Central University of Taiwan, the Space Telescope Science Institute, the National Aeronautics and Space Administration under Grant No.NNX08AR22G issued through the Planetary Science Division of the NASA Science Mission Directorate, the National Science Foundation Grant No. AST-1238877, the University of Maryland, Eotvos Lorand University (ELTE), the Los Alamos National Laboratory, and the Gordon and Betty Moore Foundation.

REFERENCES

Allaert F., Gentile G., Baes M., 2017, A&A, 605, A55
Amorisco N. C., 2017, ApJ, 844, 64
Aparicio A., Carrera R., Martínez-Delgado D., 2001, AJ, 122, 2524
Avila-Reese V., Colín P., Valenzuela O., D'Onghia E., Firmani C., 2001, ApJ, 559, 516
Balberg S., Shapiro S. L., Inagaki S., 2002, ApJ, 568, 475
Battaglia G., Helmi A., Tolstoy E., Irwin M., Hill V., Jablonka P., 2008, ApJ, 681, L13
Baur J., Palanque-Delabrouille N., Yèche C., Magneville C., Viel M., 2016, J. Cosmol. Astropart. Phys., 8, 012
Bermejo-Climent J. R. et al., 2018, MNRAS, 479, 1514
Binney J., Mamon G. A., 1982, MNRAS, 200, 361
Bode P., Ostriker J. P., Turok N., 2001, ApJ, 556, 93
Bonnivard V., Combet C., Maurin D., Walker M. G., 2015, MNRAS, 446, 3002
Bovy J., Rix H.-W., 2013, ApJ, 779, 115
Breddels M. A., Helmi A., van den Bosch R. C. E., van de Ven G., Battaglia G., 2013, MNRAS, 433, 3173
Brook C. B., Di Cintio A., 2015, MNRAS, 450, 3920
Bullock J. S., Boylan-Kolchin M., 2017, ARA&A, 55, 343
Caldwell N. et al., 2017, ApJ, 839, 20
Campbell D. J. R. et al., 2017, MNRAS, 469, 2335
Charbonnier A. et al., 2011, MNRAS, 418, 1526
Clowe D., Bradač M., Gonzalez A. H., Markevitch M., Randall S. W., Jones C., Zaritsky D., 2006, ApJ, 648, L109
Cole D. R., Dehnen W., Read J. I., Wilkinson M. I., 2012, MNRAS, 426, 601
Contenta F. et al., 2018, MNRAS, 476, 3124
D'Onghia E., Vogelsberger M., Faucher-Giguere C.-A., Hernquist L., 2010, ApJ, 725, 353
Dalcanton J. J., Hogan C. J., 2001, ApJ, 561, 35
de Blok W. J. G., 2010, Adv. Astron., 2010, 789293
Del Popolo A., 2009, ApJ, 698, 2093
Di Cintio A., Brook C. B., Macciò A. V., Stinson G. S., Knebe A., Dutton A. A., Wadsley J., 2014, MNRAS, 437, 415
Dooley G. A., Peter A. H. G., Vogelsberger M., Zavala J., Frebel A., 2016, MNRAS, 461, 710
Dotter A., Chaboyer B., Jevremović D., Kostov V., Baron E., Ferguson J. W., 2008, ApJS, 178, 89
Dubinski J., Carlberg R. G., 1991, ApJ, 378, 496
Dutton A. A., Macciò A. V., 2014, MNRAS, 441, 3359
El-Badry K., Wetzel A., Geha M., Hopkins P. F., Kereš D., Chan T. K., Faucher-Giguère C.-A., 2016, ApJ, 820, 131
El-Zant A., Shlosman I., Hoffman Y., 2001, ApJ, 560, 636
Elbert O. D., Bullock J. S., Garrison-Kimmel S., Rocha M., Oñorbe J., Peter A. H. G., 2015, MNRAS, 453, 29
Evans N. W., Sanders J. L., Geringer-Sameth A., 2016, Phys. Rev. D, 93, 103512
Farrow D. J. et al., 2014, MNRAS, 437, 748
Flewelling H. A. et al., 2016, preprint (arXiv:1612.05243)
Flores R. A., Primack J. R., 1994, ApJ, 427, L1
Foreman-Mackey D., Hogg D. W., Lang D., Goodman J., 2013, PASP, 125, 306
Gaia Collaboration et al., 2018, A&A, 616, A12
Gajda G., Łokas E. L., 2016, ApJ, 819, 20
Genina A. et al., 2018, MNRAS, 474, 1398
Gnedin O. Y., Zhao H., 2002, MNRAS, 333, 299
Goerdt T., Moore B., Read J. I., Stadel J., Zemp M., 2006, MNRAS, 368, 1073
Goerdt T., Moore B., Read J. I., Stadel J., 2010, ApJ, 725, 1707
Harvey D., Massey R., Kitching T., Taylor A., Tittley E., 2015, Science, 347, 1462
Henon M., 1970, A&A, 9, 24
Holmberg E., 1941, ApJ, 94, 385
Hu W., Barkana R., Gruzinov A., 2000, Phys. Rev. Lett., 85, 1158
Jardel J. R., Gebhardt K., Fabricius M. H., Drory N., Williams M. J., 2013, ApJ, 763, 91
Jeans J. H., 1922, MNRAS, 82, 122
Kaplinghat M., Keeley R. E., Linden T., Yu H.-B., 2014, Phys. Rev. Lett., 113, 021302
Kaplinghat M., Tulin S., Yu H.-B., 2016, Phys. Rev. Lett., 116, 041302
Kauffmann G., 2014, MNRAS, 441, 2717
Kazantzidis S., Mayer L., Mastropietro C., Diemand J., Stadel J., Moore B., 2004, ApJ, 608, 663
Keenan D. W., Innanen K. A., 1975, AJ, 80, 290
Kleyna J. T., Wilkinson M. I., Evans N. W., Gilmore G., 2001, ApJ, 563, L115
Klypin A. A., Trujillo-Gomez S., Primack J., 2011, ApJ, 740, 102
Kowalczyk K., Łokas E. L., Kazantzidis S., Mayer L., 2013, MNRAS, 431, 2796
Kowalczyk K., Lokas E. L., Valluri M., 2018, MNRAS, 476, 2918
Kravtsov A. V., 2013, ApJ, 764, L31
Kuzio de Naray R., Kaufmann T., 2011, MNRAS, 414, 3617
Laporte C. F. P., Peñarrubia J., 2015, MNRAS, 449, L90
Laporte C. F. P., Walker M. G., Peñarrubia J., 2013, MNRAS, 433, L54
Leaman R. et al., 2012, ApJ, 750, 33
Łokas E. L., 2009, MNRAS, 394, L102
Lovell M. R., Frenk C. S., Eke V. R., Jenkins A., Gao L., Theuns T., 2014, MNRAS, 439, 300
Macciò A. V., Paduroiu S., Anderhalden D., Schneider A., Moore B., 2012, MNRAS, 424, 1105
Madau P., Shen S., Governato F., 2014, ApJ, 789, L17
Mamon G. A., Łokas E. L., 2005, MNRAS, 362, 95
Martin N. F., de Jong J. T. A., Rix H.-W., 2008, ApJ, 684, 1075
Mashchenko S., Wadsley J., Couchman H. M. P., 2008, Science, 319, 174
Massari D., Breddels M. A., Helmi A., Posti L., Brown A. G. A., Tolstoy E., 2018, Nat. Astron., 2, 156
McConnachie A. W., 2012, AJ, 144, 4
Merrifield M. R., Kent S. M., 1990, AJ, 99, 1548
Merritt D., Graham A. W., Moore B., Diemand J., Terzić B., 2006, AJ, 132, 2685
Moore B., 1994, Nature, 370, 629
Navarro J. F., Eke V. R., Frenk C. S., 1996a, MNRAS, 283, L72
Navarro J. F., Frenk C. S., White S. D. M., 1996b, ApJ, 462, 563
Nipoti C., Binney J., 2015, MNRAS, 446, 1820
Oman K. A., Marasco A., Navarro J. F., Frenk C. S., Schaye J., Benítez-Llambay A., 2017, preprint (arXiv:1706.07478)
Oñorbe J., Boylan-Kolchin M., Bullock J. S., Hopkins P. F., Kereš D., Faucher-Giguère C.-A., Quataert E., Murray N., 2015, MNRAS, 454, 2092
Pascale R., Posti L., Nipoti C., Binney J., 2018, MNRAS, 480, 927
Peebles P. J. E., 2000, ApJ, 534, L127
Peñarrubia J., Pontzen A., Walker M. G., Koposov S. E., 2012, ApJ, 759, L42

Pineda J. C. B., Hayward C. C., Springel V., Mendes de Oliveira C., 2017, MNRAS, 466, 63
Planck Collaboration et al., 2014, A&A, 571, A16
Pontzen A., Governato F., 2012, MNRAS, 421, 3464
Pontzen A., Governato F., 2014, Nature, 506, 171
Pontzen A., Roškar R., Stinson G. S., Woods R., Reed D. M., Coles J., Quinn T. R., 2013, pynbody: Astrophysics Simulation Analysis for Python
Read J. I., Gilmore G., 2005, MNRAS, 356, 107
Read J. I., Steger P., 2017, MNRAS, 471, 4541
Read J. I., Wilkinson M. I., Evans N. W., Gilmore G., Kleyna J. T., 2006a, MNRAS, 366, 429
Read J. I., Wilkinson M. I., Evans N. W., Gilmore G., Kleyna J. T., 2006b, MNRAS, 367, 387
Read J. I., Lake G., Agertz O., Debattista V. P., 2008, MNRAS, 389, 1041
Read J. I., Agertz O., Collins M. L. M., 2016a, MNRAS, 459, 2573
Read J. I., Iorio G., Agertz O., Fraternali F., 2016b, MNRAS, 462, 3628
Read J. I., Iorio G., Agertz O., Fraternali F., 2017, MNRAS, 467, 2019
Rhee G., Valenzuela O., Klypin A., Holtzman J., Moorthy B., 2004, ApJ, 617, 1059
Richardson T., Fairbairn M., 2014, MNRAS, 441, 1584
Robertson A. et al., 2018, MNRAS, 476, L20
Robin A. C., Reylé C., Derrière S., Picaud S., 2003, A&A, 409, 523
Robles V. H. et al., 2017, MNRAS, 472, 2945
Rocha M., Peter A. H. G., Bullock J. S., Kaplinghat M., Garrison-Kimmel S., Oñorbe J., Moustakas L. A., 2013, MNRAS, 430, 81
Rojas-Niño A., Read J. I., Aguilar L., Delorme M., 2016, MNRAS, 459, 3349
Schive H.-Y., Chiueh T., Broadhurst T., 2014, Nature Phys., 10, 496
Schneider A., Trujillo-Gomez S., Papastergis E., Reed D. S., Lake G., 2017, MNRAS, 470, 1542
Shao S., Gao L., Theuns T., Frenk C. S., 2013, MNRAS, 430, 2346
Sharma S., Bland-Hawthorn J., Johnston K. V., Binney J., 2011, ApJ, 730, 3
Sohn S. T., Patel E., Besla G., van der Marel R. P., Bullock J. S., Strigari L. E., van de Ven G., Walker M. G., 2017, ApJ, 849, 93
Sparre M., Hayward C. C., Feldmann R., Faucher-Giguère C.-A., Muratov A. L., Kereš D., Hopkins P. F., 2017, MNRAS, 466, 88
Spergel D. N., Steinhardt P. J., 2000, Phys. Rev. Lett., 84, 3760
Springel V., Frenk C. S., White S. D. M., 2006, Nature, 440, 1137
Springel V. et al., 2008, MNRAS, 391, 1685
Stadel J. G., 2001, Ph.D. Thesis, Univ. Washington
Stadel J., Potter D., Moore B., Diemand J., Madau P., Zemp M., Kuhlen M., Quilis V., 2009, MNRAS, 398, L21
Strigari L. E., Bullock J. S., Kaplinghat M., 2007, ApJ, 657, L1
Teyssier R., Pontzen A., Dubois Y., Read J. I., 2013, MNRAS, 429, 3068
Valenzuela O., Rhee G., Klypin A., Governato F., Stinson G., Quinn T., Wadsley J., 2007, ApJ, 657, 773
Valli M., Yu H.-B., 2017, preprint (arXiv:1711.03502)
van den Bosch F. C., Ogiya G., Hahn O., Burkert A., 2018, MNRAS, 474, 304
van der Marel R. P., 1994, MNRAS, 270, 271
Vogelsberger M., Zavala J., Loeb A., 2012, MNRAS, 423, 3740
Walker M. G., Peñarrubia J., 2011, ApJ, 742, 20
Walker M. G., Olszewski E. W., Mateo M., 2015a, MNRAS, 448, 2717
Walker M. G., Olszewski E. W., Mateo M., 2015b, MNRAS, 448, 2717
Wheeler C. et al., 2017, MNRAS, 465, 2420
Wilson A. G., 1955, PASP, 67, 27
Zavala J., Vogelsberger M., Walker M. G., 2013, MNRAS, 431, L20
Zhu L., van de Ven G., Watkins L. L., Posti L., 2016, MNRAS, 463, 1117

APPENDIX A: EXAMPLE GRAVSPHERE MODEL FITS

In this Appendix, we show example GRAVSPHERE model fits for the real Draco data and the Mock–Cusp and Mock–Core mocks. (The fit for the Mock–CoreDen mock is comparably good and so we omit this for brevity.) The results are shown in Fig. A1, where the panels show from left to right: the projected stellar velocity dispersion profile; the surface brightness profile of the stars; and the 'Virial Shape Parameters', v_{s1} (equation (17)) and v_{s2} (equation (19)). The grey contours show the 68 per cent (dark) and 95 per cent (light) confidence intervals of the GRAVSPHERE model chains. The data points mark the input data used for the model fits.

For both the mock data and the real Draco data, the GRAVSPHERE models recover the input data within the error bars. In Read & Steger (2017) we found, using mock data, that when unmodelled triaxiality caused significant bias in the models, this manifested also in a poor fit to either v_{s1} or v_{s2}. This does not appear to be the case for Draco.

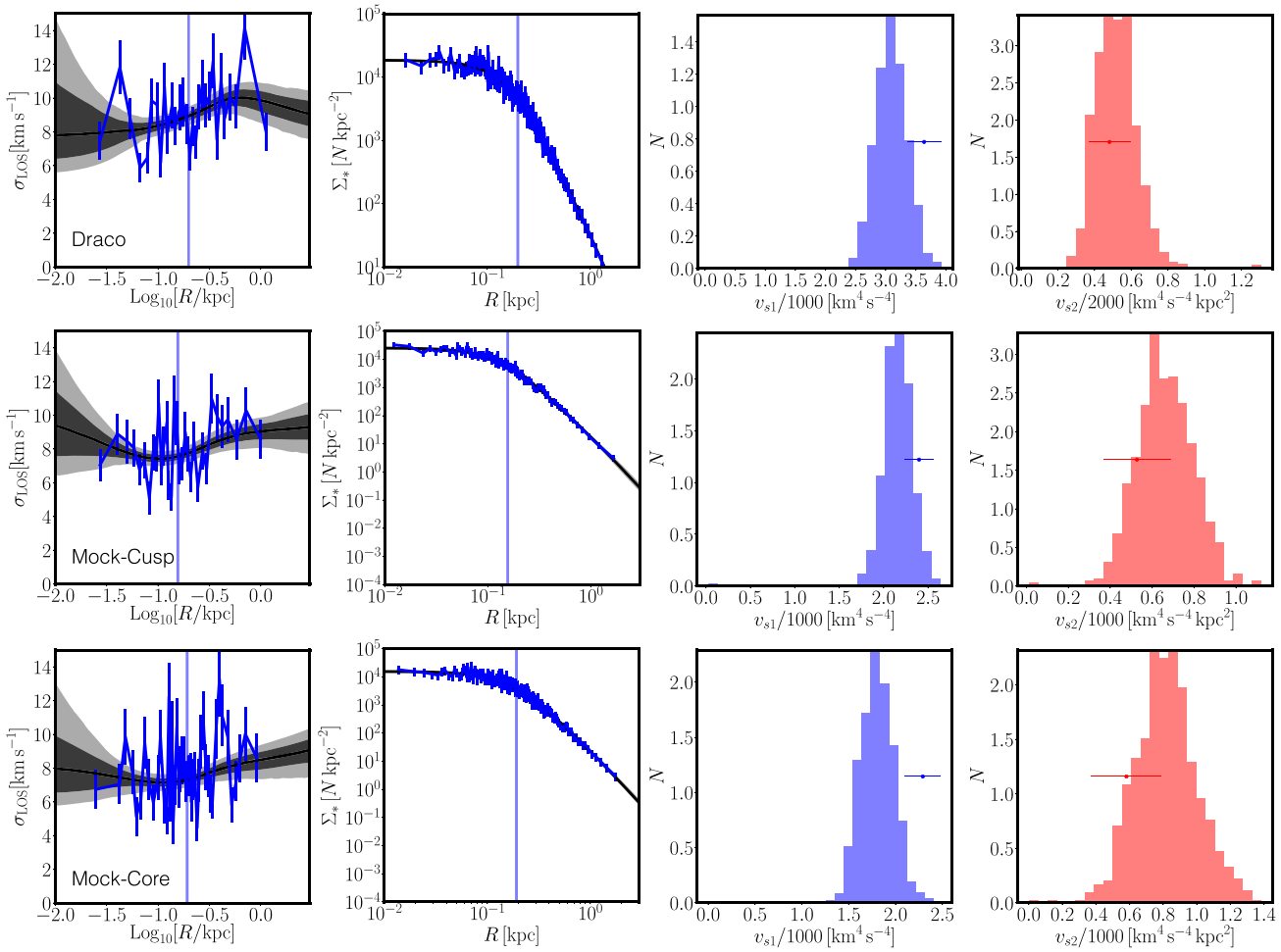

Figure A1. Example GravSphere model fits for Draco (top), the Mock–Cusp mock (middle) and the Mock–Core mock (bottom). The panels show, from left to right: the projected stellar velocity dispersion profile; the surface brightness profile of the stars; and the 'Virial Shape Parameters', v_{s1} (equation (17)) and v_{s2} (equation (19)). The grey contours show the 68 per cent (dark) and 95 per cent (light) confidence intervals of the GravSphere model chains. The data points mark the input data used for the model fits. Notice that the errors on v_{s1} and v_{s2} are comparable for the real Draco data and the mock, despite the mock having more kinematic tracers. This occurs because the mock data have a steeply rising $\langle v^4_{\rm LOS}\rangle$ to large R, unlike the true Draco data (see the text and Section 3 for further details).

APPENDIX B: TESTING THE EFFECT OF BINARY STARS, FOREGROUND CONTAMINATION AND SPECTROSCOPIC SAMPLE SIZE

In this Appendix, we explore the effects of binary stars, foreground contamination, and the spectroscopic sample size on the Mock–Core mock. The results are shown in Fig. B1, where the lines and contours are as in Fig. 4. The top row shows how the results change when doubling the spectroscopic sample size to 1000 stars. Now the slight bias towards cuspy models seen in Fig. 4 (middle row) is gone. However, some bias in the recovered velocity anisotropy profile (Fig. B1, too row, right panel) remains. The bottom row shows what happens if we increase the spectroscopic sample size further to 2000 stars and remove the binary stars and foreground contamination. The results for the density profile further improve, while now there is only some weak bias towards radial anisotropy at the centre (Fig. B1, bottom row, right-hand panel). These tests demonstrate that both the uncertainty and bias in the recovery of the dark matter density profile depend primarily on the spectroscopic sample size. Binary stars and foreground contamination induce some small bias, particularly in the velocity anisotropy profile, but their effect is largely benign.

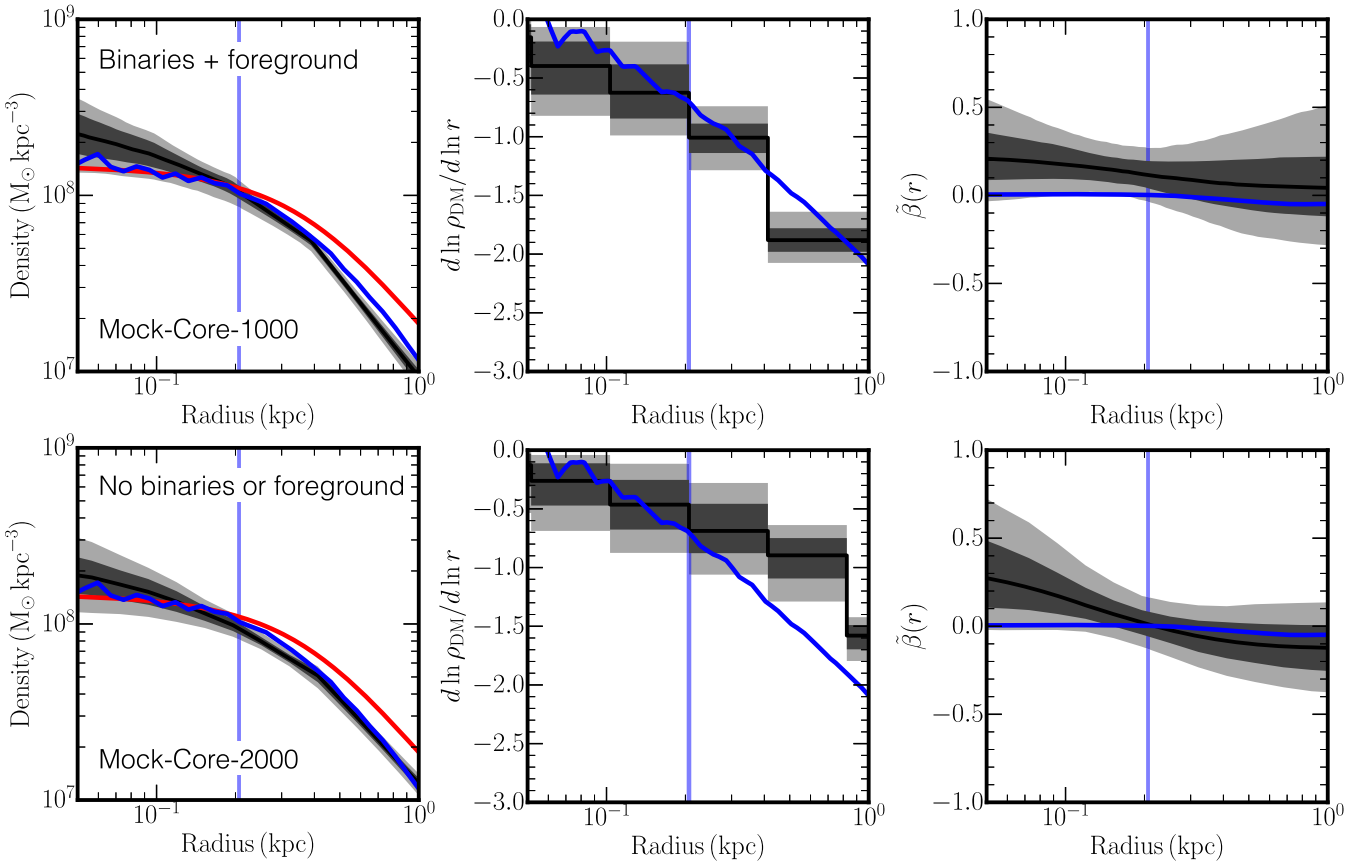

Figure B1. As Fig. 4 for the Mock–Core mock, but with 1000 stars with spectroscopic data (top) and with 2000 stars with spectroscopic data but without binary stars or foreground contamination (bottom).

APPENDIX C: TESTING THE ROBUSTNESS OF OUR GRAVSPHERE MODELS FOR DRACO

In this Appendix, we explore the robustness of our GRAVSPHERE models for Draco. In Fig. C1 (left-hand panel), we show results for GRAVSPHERE models run without VSPs (blue), without v_{s2} (purple), and with our default choice of v_{s1} + v_{s2} (black). The contours show the 95 per cent confidence intervals of the radial dark matter density profile in each case. As can be seen, the VSPs improve the constraints for $R > R_{1/2}$ and, to a lesser extent, for $R < 0.25R_{1/2}$. However, in all cases, Draco favours a large density over the range $0.5 < R/R_{1/2} < 1$, consistent with a CDM cusp.

In Fig. C1, middle and right-hand panels, we explore the effect of changing our priors on the logarithmic density slope. Our default priors allow a range $-3 < \gamma_{\rm DM} < 0$ in each mass bin. However, as pointed out in Section 4, in the absence of sufficiently constraining data, this can lead to a bias towards cuspier models (since models with a flat core, $\gamma_{\rm DM} = 0$, occupy a smaller hypervolume of the parameter space than cuspy models with $\gamma_{\rm DM} = -1$). To test the effect of this bias on our results for Draco, we re-ran our GRAVSPHERE model chains assuming a flat prior over the range $-3 < \gamma'_{\rm DM} < 2$, and setting $\gamma_{\rm DM} = 0$ if $\gamma'_{\rm DM} > 0$ and $\gamma_{\rm DM} = \gamma'_{\rm DM}$ otherwise. In the absence of constraining data, this rather extreme prior biases GRAVSPHERE towards cores by creating a large region of hypervolume in which $\gamma_{\rm DM} = 0$. As can be seen, this new prior has the effect of making Draco less steep inside $R_{1/2}$, systematically pushing $\gamma_{\rm DM}(R < R_{1/2})$ towards cores (Fig. C1, right-hand panel). As for our mock data tests in Section 4, this shift is smaller than our 68 per cent confidence intervals on $\gamma_{\rm DM}$, but is nonetheless a source of systematic uncertainty on our recovery of $\gamma_{\rm DM}(R < R_{1/2})$. By contrast, the amplitude of the inner density at 150 pc is not significantly changed. We find $\rho_{\rm DM}(150\,{\rm pc}) = 2.1^{+0.5}_{-0.6} \times 10^8\,{\rm M}_\odot\,{\rm kpc}^{-3}$, with a logarithmic slope of $\gamma_{\rm DM}(150\,{\rm pc}) = -0.70^{+0.52}_{-0.52}$ at 95 per cent confidence.

Note, as pointed out in Section 4.6, we consider the above modified prior on $\gamma_{\rm DM}$ to be rather extreme. It removed a small bias on our Mock–Core mock towards cusps while introducing a larger bias on our Mock–Cusp towards cores (Fig. 5). Nonetheless, even with this prior, our GRAVSPHERE models for Draco favour a high density and steep logarithmic slope at 150 pc, consistent with a CDM cusp (Section 2).

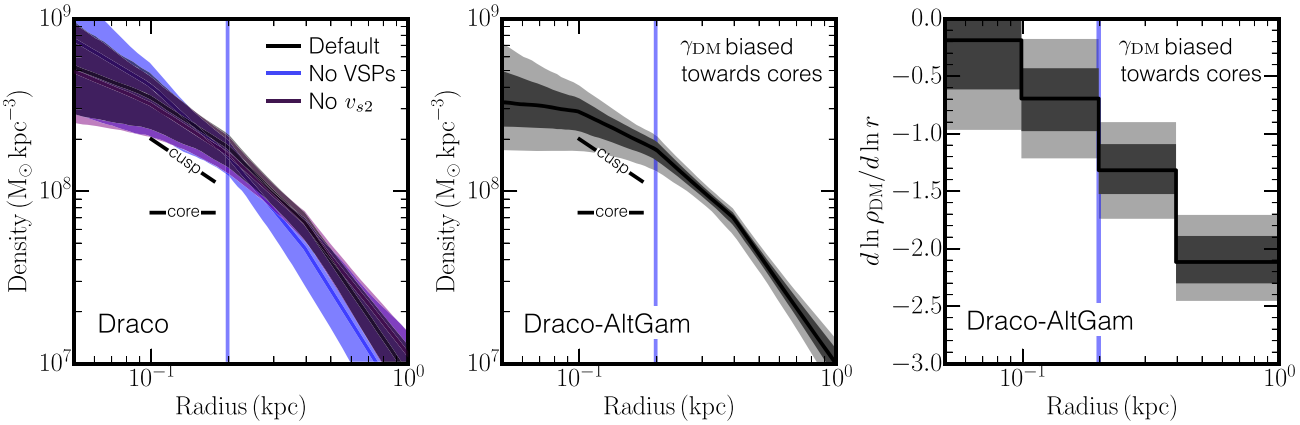

Figure C1. Testing the robustness of our GRAVSPHERE models for Draco. The left-hand panel shows the 95 per cent confidence intervals of the dark matter density profile for GRAVSPHERE models run without VSPs (blue) and without v_{s2} (purple) as compared to our default model with VSPs (black). The lines and contours are as in Fig. 7. The middle panel shows similar results for Draco with a rather extreme prior on γ_{DM} that biases the models towards dark matter cores. The right-hand panel shows $\gamma_{DM}(r) \equiv d \ln \rho_{DM}/d \ln r$ for this same model.

This paper has been typeset from a TEX/LATEX file prepared by the author.